Article

Cell Host & Microbe

Aspergillus fumigatus hijacks human p11 to redirect fungal-containing phagosomes to non-degradative pathway

Graphical abstract

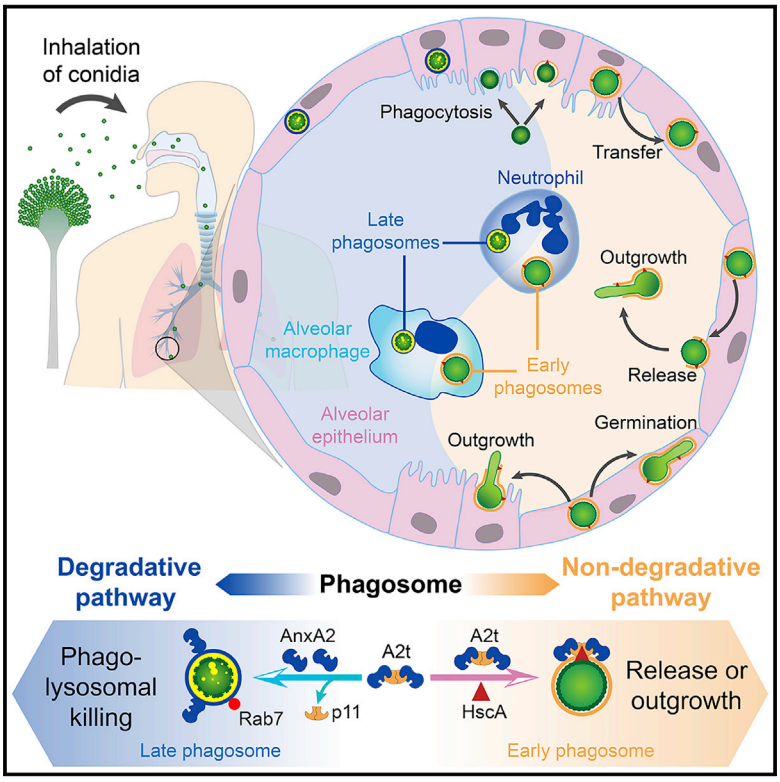

Highlights

- The human p11 protein is a regulatory node of phagosome maturation
- The HscA protein of *Aspergillus fumigatus* anchors p11 on phagosomal membranes
- p11 redirects phagosomes to the non-degradative pathway, allowing escape of conidia
- A single nucleotide polymorphism (SNP) in the p11 gene is associated with susceptibility to invasive aspergillosis

Authors

Lei-Jie Jia, Muhammad Rafiq, Lukáš Radosa, ..., Agostinho Carvalho, Olaf Kniemeyer, Axel A. Brakhage

Correspondence

axel.brakhage@leibniz-hki.de

In brief

Jia et al. discover a mechanism allowing the human-pathogenic fungus *A. fumigatus* to escape intracellular killing by human cells. The authors identify the p11 protein as a regulatory node of phagosome maturation that is targeted by *A. fumigatus*. An SNP in the p11 gene is associated with invasive aspergillosis susceptibility.

Jia et al., 2023, Cell Host & Microbe *31*, 373–388
March 8, 2023
https://doi.org/10.1016/j.chom.2023.02.002

CellPress

Cell Host & Microbe

CellPress
OPEN ACCESS

Article

Aspergillus fumigatus hijacks human p11 to redirect fungal-containing phagosomes to non-degradative pathway

Lei-Jie Jia,[1] Muhammad Rafiq,[1,2] Lukáš Radosa,[1] Peter Hortschansky,[1] Cristina Cunha,[3,4] Zoltán Cseresnyés,[5] Thomas Krüger,[1] Franziska Schmidt,[1] Thorsten Heinekamp,[1] Maria Straßburger,[6] Bettina Löffler,[7] Torsten Doenst,[8] João F. Lacerda,[9,10] António Campos, Jr.,[11] Marc Thilo Figge,[2,5] Agostinho Carvalho,[3,4] Olaf Kniemeyer,[1] and Axel A. Brakhage[1,2,12,*]

[1]Department of Molecular and Applied Microbiology, Leibniz Institute for Natural Product Research and Infection Biology (Leibniz-HKI), 07745 Jena, Germany
[2]Institute of Microbiology, Friedrich Schiller University, 07745 Jena, Germany
[3]Life and Health Sciences Research Institute (ICVS), School of Medicine, University of Minho, Campus de Gualtar, 4710-057 Braga, Portugal
[4]ICVS/3B's - PT Government Associate Laboratory, Braga/Guimarães, Portugal
[5]Research Group Applied Systems Biology, Leibniz-HKI, Jena, Germany
[6]Transfer Group Anti-infectives, Leibniz-HKI, 07745 Jena, Germany
[7]Institute of Medical Microbiology, Jena University Hospital, 07747 Jena, Germany
[8]Klinik für Herz- und Thoraxchirurgie, Jena University Hospital, 07747 Jena, Germany
[9]Serviço de Hematologia e Transplantação de Medula, Hospital de Santa Maria, 1649-035 Lisboa, Portugal
[10]Instituto de Medicina Molecular, Faculdade de Medicina da Universidade de Lisboa, 1649-028 Lisboa, Portugal
[11]Serviço de Transplantação de Medula Óssea, Instituto Português de Oncologia do Porto, 4200-072 Porto, Portugal
[12]Lead contact
*Correspondence: axel.brakhage@leibniz-hki.de
https://doi.org/10.1016/j.chom.2023.02.002

SUMMARY

The decision whether endosomes enter the degradative or recycling pathway in mammalian cells is of fundamental importance for pathogen killing, and its malfunctioning has pathological consequences. We discovered that human p11 is a critical factor for this decision. The HscA protein present on the conidial surface of the human-pathogenic fungus *Aspergillus fumigatus* anchors p11 on conidia-containing phagosomes (PSs), excludes the PS maturation mediator Rab7, and triggers binding of exocytosis mediators Rab11 and Sec15. This reprogramming redirects PSs to the non-degradative pathway, allowing *A. fumigatus* to escape cells by outgrowth and expulsion as well as transfer of conidia between cells. The clinical relevance is supported by the identification of a single nucleotide polymorphism in the non-coding region of the *S100A10* (p11) gene that affects mRNA and protein expression in response to *A. fumigatus* and is associated with protection against invasive pulmonary aspergillosis. These findings reveal the role of p11 in mediating fungal PS evasion.

INTRODUCTION

A fundamental question of cell biology is the molecular understanding of the sorting of internalized cargo, including the decision whether endosomes enter the degradative or non-degradative recycling pathway. In the non-degradative pathway, cargos are redirected to the cell surface, secreted to the environment, maintained in intracellular vesicles, or transferred to other cells.[1–4] Erroneous decisions in endosomal sorting are associated with various diseases, including neurological and immunological disorders as well as cancer.[5] The investigation of pathogens that interfere with phagosome maturation is important to understand pathogenesis but also helps to identify host proteins that control the fate of endosomes.[6–9] To date, there is limited knowledge about proteins that are decisive for directing endosomes to the degradative or secretory pathways.[10,11]

A prominent example of a pathogen that modulates maturation and activity of phagosomes is the fungal pathogen *Aspergillus fumigatus* that can cause disseminated infections.[12–15] Conidia are released into the air and are continuously inhaled. In the lung, conidia can survive in the phagosomes of immune cells as well as epithelial cells for some time.[16–19] Similar strategies of evading the host immune system have been described for several bacterial and fungal pathogens.[20,21] For many microbial pathogens, this process is linked to the secretion of effector proteins that interfere with the host's membrane trafficking system.[7,8] For *A. fumigatus*, we previously established that the conidial pigment dihydroxynaphthalene (DHN) melanin prevents

the formation of functional phagolysosomes.[18,19] DHN melanin sequesters Ca^{2+} and thus prevents LC3-associated phagocytosis via interference with calcium-calmodulin dependent signaling pathways[22] and reduces the formation of lipid-raft microdomains in the phagosomal membrane that are essential for fully functional phagolysosomes.[9] We were intrigued by the observation that some non-melanized mutant conidia still escaped killing by phagocytes,[9,23] indicating that additional mechanisms might be involved in the immune escape of this pathogen.

We discovered a strategy of this fungal pathogen of evading the host immune system by redirecting conidia-containing phagosomes toward exocytosis and the release of conidia. This is mediated by the specific interaction of the fungal surface protein HscA with the human p11 protein (also called S100A10 or light chain of annexin A2 [AnxA2]). We show that p11 is a decisive regulatory node for directing endosomes to different pathways.

RESULTS

Surface-exposed HscA protein of *A. fumigatus* binds to host epithelial cells

We used a strategy for identifying microbial surface proteins that bind to host epithelial cells by biotinylation[24] coupled with affinity purification (Figure 1A).[25] Immunofluorescence imaging revealed that protein extracts of germlings, but not dormant conidia or mycelia, led to labeling of the surface of A549 cells (Figure 1B). To identify the interacting proteins, we isolated proteins of A549 cells after their incubation with *A. fumigatus* protein extracts. By western blot analysis, we identified a candidate protein with a molecular mass of 70 kDa present in protein extracts of germlings and, with a weaker signal, swollen conidia (Figures 1C and 1D). Among the six proteins with a molecular mass of about 70 kDa detected in germlings,[24] only the heat shock protein HscA was predominantly identified in germling samples. Indeed, the mRNA level of the *hscA* gene was upregulated in swollen conidia (Figure 1E), as were the protein levels of HscA in swollen conidia and germlings (Figure 1F). To investigate a potential conidial surface localization of HscA, we generated an *hscA-myc* strain of *A. fumigatus* (Figures S1A and S1C–E). HscA-Myc was clearly identified on the surface of germlings (Figure 1G).

To provide additional evidence, we incubated N-terminal Twin-Strep-tagged recombinant HscA (rHscA) and Hsp70 (rHsp70) with A549 cells, which revealed that rHscA, but not rHsp70, bound to A549 cells (Figures 1H and 1I). Further evidence for binding was obtained by incubation of A549 cells with protein extracts of an *hscA-gfp* strain (Figures S1A, S1B, and S1E–H). After immunostaining, HscA-GFP was detected on the surface of A549 cells, unlike the CcpA-GFP control, which is also a conidial surface protein (Figures S1I and S1J).[26] Although the heat shock protein Hsp70 was found on the surface of *hscA-gfp* dormant conidia (Figure S1H), binding of Hsp70 to A549 cells was not observed (Figure S1I). We also detected binding of rHscA to several other epithelial cells, including human bronchial epithelial (BEAS-2B), lung epithelial (H441), and liver epithelial (HepG2) cells, and mouse type-II lung epithelial (T7) cells (Figure 1J). Collectively, these results show that surface-exposed heat shock protein HscA of *A. fumigatus* binds to mouse and human epithelial cells.

HscA is an adhesin and effector protein that interferes with phagosome maturation

To explore the possible role of HscA in pathogen-host interaction, we generated an *hscA* deletion mutant (Δ*hscA*) (Figures S1A–D) that produced slightly smaller colonies (Figures S1K and S1L) but had no obvious defects in sporulation and germination of conidia, nor an altered susceptibility against various stressors compared with wild-type (WT) strains (Figures S1M–O). Its minor growth defect could be restored by complementation of Δ*hscA* with the *hscA-myc* or *hscA* gene (Figures S1K–O).

Based on its binding ability, we considered the potential for an effector function of HscA. In a lactate dehydrogenase (LDH) release assay, Δ*hscA* caused significantly less damage to host cells than WT conidia (Figure 2A). Addition of purified rHscA or rHsp70 did not impact LDH release from A549 cells without infection, whereas addition of rHscA, but not rHsp70, increased LDH release from A549 cells infected with Δ*hscA* to levels seen with WT conidia. Thus, addition of rHscA compensated for the Δ*hscA* phenotype (Figure 2A), which suggests that HscA contributes to the cell damage caused by *A. fumigatus*. In support of a function as adhesin for HscA, the association of Δ*hscA* conidia with A549 cells was reduced compared with WT conidia (Figure 2B). This reduction was abolished by adding rHscA, but not rHsp70 (Figure 2B).

Since *A. fumigatus* conidia are internalized by alveolar epithelial cells and targeted to phagolysosomes,[16,27] we assessed internalization and intracellular processing of conidia. After 8 h of incubation, a similar proportion of 12%–15% of WT and Δ*hscA* conidia were internalized by A549 cells irrespective of whether rHscA or rHsp70 were added (Figure 2C). Interestingly, approximately 2-fold more Δ*hscA* than WT conidia ended up in acidified phagosomes (Figures 2D and 2E). Addition of rHscA, but not rHsp70, reduced the amount of Δ*hscA* conidia in acidified phagosomes (Figure 2D). Another marker for the maturation of phagosomes is the assembly of the NADPH oxidase complex, consisting of p47phox and other cytosolic subunits, on the phagosomal membrane.[22,23] 25% of WT and 48% of Δ*hscA* conidia were localized in p47phox-positive ($p47phox^+$) phagosomes (Figures 2F and 2G), which further supports the role of HscA in inhibiting the maturation of phagosomes. We also analyzed phagosomes for presence of Rab7 (Figure 2H), which plays an essential role in phagosome maturation.[28–30] While 46% of phagosomes containing WT conidia were Rab7-positive ($Rab7^+$), the proportion increased to 73% when phagosomes contained Δ*hscA* conidia (Figure 2I). Addition of rHscA, but not rHsp70, reduced the percentage of Δ*hscA* conidia in $Rab7^+$ phagosomes (Figure 2I), possibly due to binding of rHscA to the surface of Δ*hscA* conidia (Figure 2H). 48% of internalized WT germlings were located in $Rab7^+$ phagosomes of A549 cells; this increased to 75% for germinated Δ*hscA* conidia (Figures 2H and 2J). The addition of rHscA or rHsp70 protein did not alter this percentage (Figure 2J), suggesting that HscA on the conidial surface prevents recruitment of Rab7 to phagosomes.

To further investigate if the inhibition of phagosome maturation is due to HscA, we generated latex beads coated with rHscA, rHsp70, or BSA as control (Figure 2K). A strong signal of Rab7 was detected on phagosomes containing BSA beads, whereas only faint staining of Rab7 on phagosomes

CellPress
OPEN ACCESS

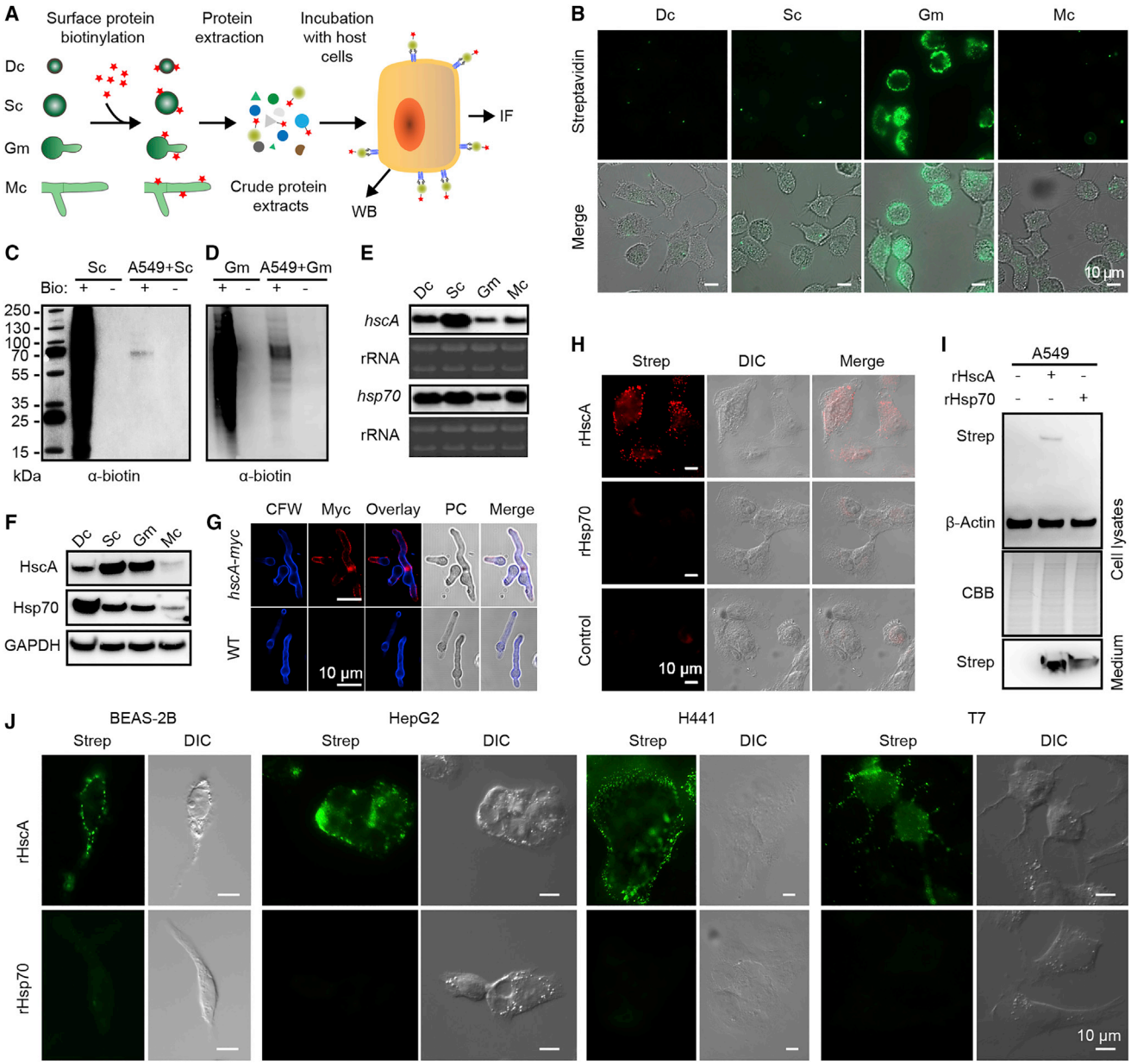

Figure 1. Fungal surface protein HscA binds to the surface of host cells

(A) Scheme illustrating the experimental set-up used for experiments shown in (B–D). Abbreviations: Dc, dormant conidia; Sc, swollen conidia; Gm, germlings; Mc, mycelia; IF, immunofluorescence analysis; WB, western blot analysis.

(B) Biotinylated *A. fumigatus* surface protein binds to the surface of host cells.

(C and D) Detection of biotinylated proteins from protein extracts of *A. fumigatus* (C) Sc and (D) Gm that bind to host cells. Protein extracts from *A. fumigatus* conidia with (Bio +) or without (Bio -) biotinylation were added to A549 cells.

(E) *hscA* expression is up-regulated in Sc. Total RNA of WT *A. fumigatus* Dc, Sc, Gm, and Mc was analyzed using northern blotting.

(F) The HscA protein level increased in Sc and Gm.

(G) Immunofluorescence detection of HscA-Myc on the surface of *A. fumigatus* germlings. CFW, calcofluor white; PC, phase contrast.

(H–J) Recombinant HscA (rHscA) binds to host cells. See also Figures S1F–J. (H) Binding of rHscA to A549 cells was detected by immunostaining of cells with anti-strep antibody. DIC, differential interference contrast. (I) Detection of rHscA from protein extracts of A549 cells by immunoblotting. CBB, Coomassie brilliant blue staining. (J) rHscA binds to human BEAS-2B, H441, and HepG2 cells and mouse T7 cells.

Scale bars, 10 μm.

containing rHscA beads was observed (Figure 2L). Accordingly, coating of Δ*hscA* conidia with rHscA protein blocked recruitment of Rab7 to phagosomes (Figure 2H). Because attachment or internalization of rHsp70 beads was a rare event (Figure 2M), we also compared the association of coated latex beads with host cells. As expected, rHscA

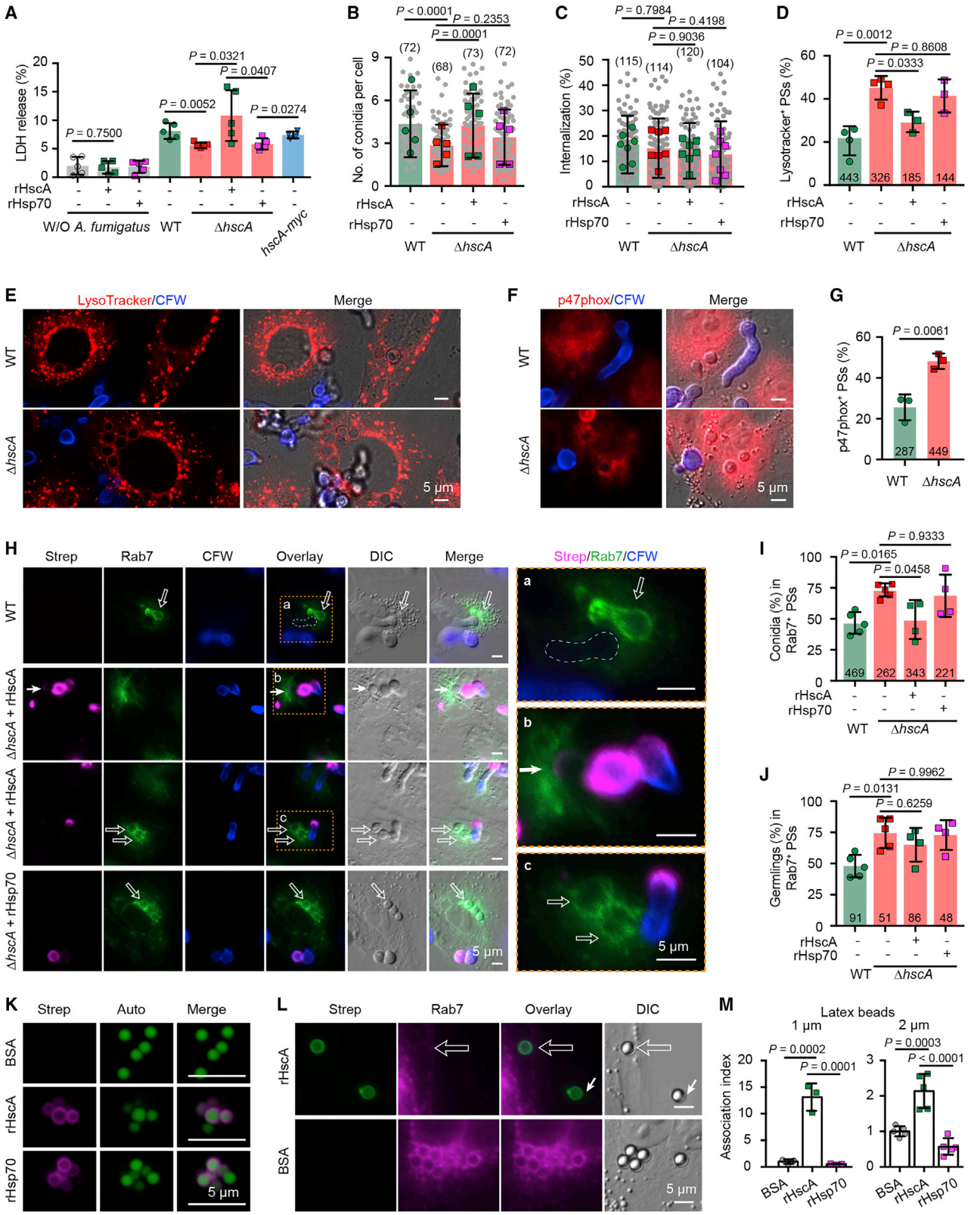

Figure 2. HscA functions as an effector protein

(A) Relative LDH release of A549 cells incubated with conidia of the indicated strains. Control cells were incubated with proteins only and without (W/O) *A. fumigatus*.

(legend continued on next page)

significantly increased the association of latex beads to A549 cells compared with rHsp70- or BSA-coated beads (Figures 2M). Overall, these data indicate that HscA mediates adhesion of conidia to host cells and prevents maturation of conidia-containing phagosomes.

HscA targets the human host p11 protein

By applying immunostaining assays, we learned that binding of HscA to A549 cells was sensitive to trypsin degradation (Figure S2A) and to fixation of cells with formaldehyde (Figure S2B). To identify the thus predicted proteinaceous binding partner, protein extracts of A549 cells were incubated with rHscA or rHsp70 for affinity purification. Co-purified proteins were analyzed using LC-MS/MS (Figure S2C). Between 95 and 226 human proteins were exclusively found in samples co-purified with rHscA or both rHscA and rHsp70 (Figure 3A; Table S1). In eluates of all purifications, p11 (S100A10) was co-purified (Figures 3A and 3B; Table S1). p11 is known to form a heterotetramer (A2t) with AnxA2 and is thereby protected from degradation.[31,32] However, AnxA2 was detected in all samples irrespective of the presence of rHscA (Figure 3B) and does not seem to be targeted by HscA. Immunofluorescence analysis further revealed colocalization of HscA-Myc with p11 on the surface of A549 cells (Figure 3C).

To further substantiate that binding of HscA to host cells is p11-dependent, we generated a p11-knockout A549 cell line (p11-KO) (Figures S3A and S3B). As expected, rHscA was not detected on the surface of p11-KO cells (Figure 3D). To assess whether HscA targets p11 in A549 cells, we incubated A549 cells with protein extracts from WT or *hscA-gfp* strain. After incubation, HscA and HscA-GFP were detected in the A549 lysates (Figure 3E). Importantly, p11 together with AnxA2 were co-precipitated with HscA-GFP (Figure 3E). These results strongly suggest that p11 is a target of HscA, most likely as part of a complex with A2t.

p11 participates in adherence and phagocytosis of *A. fumigatus* conidia

To further investigate the role of p11 in HscA-mediated adhesion and phagocytosis, we examined the subcellular localization of the proteins in A549 cells infected with conidia. p11 and AnxA2 were both detected at the cytoplasmic membrane as previously reported.[33,34] Both proteins were also present on phagocytic cups (Figures 3F, S3C, and S4A) and phagosomes containing conidia (Figures 3G and S4A). Although p11 was present on phagocytic cups containing Δ*hscA* conidia (Figure 3F), quantification revealed that 74% of WT and only 53% of Δ*hscA* conidia were associated with p11-positive ($p11^+$) phagocytotic structures (Figure 3H). This reduction was abolished by adding rHscA, but not rHsp70, to the co-incubation of A549 cells with Δ*hscA* conidia (Figure 3H).

Since accumulation of p11 on phagocytic cups suggested a role of p11 for phagocytosis of conidia, we employed p11-KO cells. As expected, there were fewer WT conidia associated with p11-KO cells than control A549-Cas9 cells. The A549-Cas9 cells behaved like the A549 cells, as more WT conidia than Δ*hscA* conidia were associated with these cells (Figure 3I). The association of WT conidia with p11-KO cells was similar to that observed with Δ*hscA* with A549-Cas9 cells or p11-KO cells. In agreement with the previous result that HscA did not affect the internalization of conidia in A549 cells (Figure 2C), deletion of p11 did not affect internalization of conidia (Figure 3J).

p11 protein abundance is increased upon *A. fumigatus* infection

After incubation with conidia, the fluorescence signal indicative of the presence of p11 in A549 cells having close contact with conidia was stronger than in cells without conidial contact (Figures 3K and S4B). Furthermore, a stronger intensity of p11 immunofluorescence and more $p11^+$ granules were observed in infected compared with uninfected A549 cells (Figures 3K, S4B, and S4C). This was due to increased p11 levels after incubation of A549 cells with WT and Δ*hscA* conidia (Figures 3L and S4D). Thus, HscA itself is not responsible for the induction of p11 production. The amount of AnxA2 did not change during the incubation (Figures 3L and S4D) and was not affected by the knockout or knockdown of p11 (Figures S3B and S4E). Collectively, our data indicate that the amount of p11, but not AnxA2, increases upon contact of cells with *A. fumigatus* conidia.

HscA-induced presence of p11 on phagosomes prevents phagosomal maturation

AnxA2 is present on endosomes and plays a role in early-to-late phagosome transition.[35,36] Morel and Gruenberg did not detect

(B and C) (B) Association and (C) internalization of *A. fumigatus* conidia with/by A549 cells. Gray dots indicate the calculated values of individual microscopic images and colored dots indicate the mean of individual experiments.

(D–G) HscA prevents phagosome (PS) maturation. (D) Percentage of acidified PSs containing conidia of WT or Δ*hscA*. (E and F) Microscopy images of (E) LysoTracker$^+$ or (F) p47phox$^+$ PSs of A549 cells containing conidia. Extracellular conidia were stained with CFW. (G) Percentage of p47phox$^+$ PSs of A549 cells containing conidia.

(H–J) HscA prevents Rab7 recruitment to PSs containing *A. fumigatus* conidia. (H) Immunofluorescence staining of Rab7$^+$ PSs of A549 cells containing WT or Δ*hscA* conidia. Δ*hscA* conidia were incubated with rHscA or rHsp70 proteins before inoculation. Open and thin arrows indicate conidia in Rab7$^+$ PSs and a Rab7-negative PS containing Δ*hscA* conidia coated with rHscA, respectively. Regions labeled with a, b, and c in dashed-line boxes are magnified on the right. Dashed-line circle marks a Rab7-negative PS containing germinated WT conidia.

(I and J) Percentage of Rab7$^+$ PSs containing *A. fumigatus* conidia (I) or germlings (J).

(K–M) rHscA prevents Rab7 recruitment to PSs that contain latex beads and contributes to association of latex beads with host cells. (K) Immunofluorescence staining of green autofluorescent (Auto) latex beads coated with recombinant proteins. BSA, bovine serum albumin. (L) Immunofluorescence staining of A549 cells with PSs containing latex beads. The open arrow indicates a phagocytosed latex bead coated with rHscA; the solid arrow marks an extracellular latex bead. (M) Association index of latex beads with a diameter of 1 μm or 2 μm associated with A549 cells.

Statistics: error bars represent the mean ± SD; p values are calculated by unpaired, two-tailed t test (A and G) or one-way ANOVA followed by Tukey's multiple comparisons test (B, C, D, I, J, and M).

Scale bars, 5 μm.

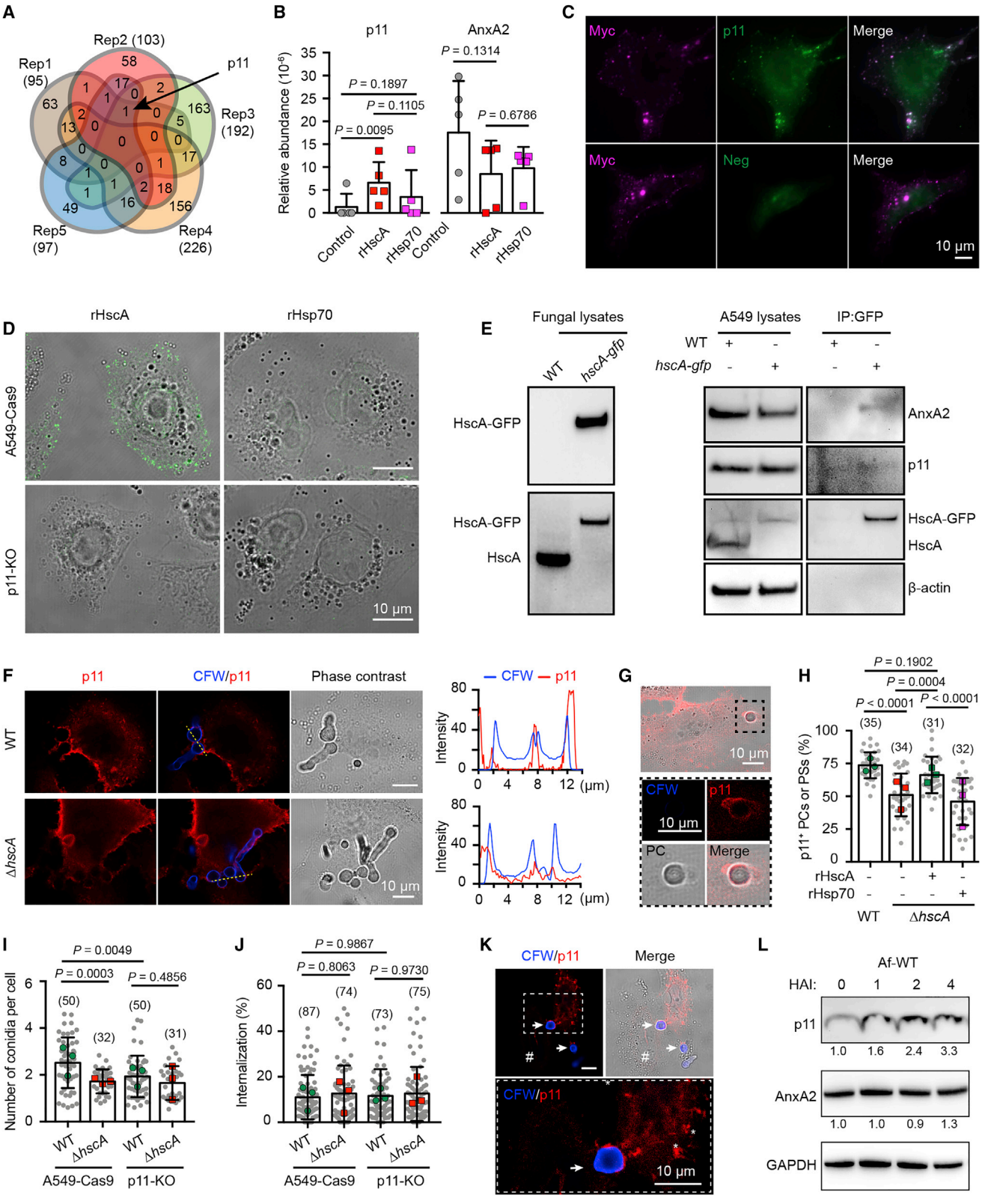

(legend on next page)

p11 on endosomes and postulated it to be dispensable for AnxA2 association to endosomes.[37] We found that although AnxA2 was detected on p11$^+$ phagocytic cups and phagosomes (Figure S4A), p11 was only observed on a few AnxA2-positive (AnxA2$^+$) phagosomes containing WT conidia (Figure 4A). Compared with WT, more Δ*hscA* conidia were found in AnxA2$^+$/p11$^-$ phagosomes (Figures 4A and 4B). This agrees with the observation that more than 60% of WT and Δ*hscA* conidia were found in AnxA2$^+$/p11$^-$ phagosomes of p11-knockdown (p11-KD) cells (Figure 4B). Based on the high percentage of p11$^+$ phagocytic cups containing WT conidia (Figure 3H), we hypothesize that HscA plays a role in stabilizing A2t on phagosomes. To test this, we incubated A549 cells with magnetic latex beads coated with rHscA or rHsp70 and isolated beads-containing phagosomes.[38] Immunoblotting confirmed that AnxA2 was eluted from both rHscA- and rHsp70-coated beads. However, p11 was only eluted from rHscA-coated beads (Figure 4C). We also applied the chemical inhibitor A2ti-1, which inhibits binding of AnxA2 to p11,[39,40] to A549 cells before infection. A549 cells treated with A2ti-1 showed a significantly reduced proportion of p11$^+$ phagocytic cups and phagosomes (Figures 4D and 4E) irrespective of the presence of HscA on conidia. Overall, these results confirm that HscA plays a role in stabilizing A2t on the phagosomal membrane.

The presence of HscA on conidia reduced staining for Rab7 (Figures 2H–2J), suggesting that interaction of HscA and A2t on phagosomes inhibits phagosome maturation. As expected, there was no Rab7 signal on p11$^+$ phagosomes (Figure 4F). Although a weak p11 signal was detectable at the interface between the cytoplasmic membrane and extracellular Δ*hscA* germlings, very few Δ*hscA* conidia were localized in p11$^+$ phagosomes (Figure 4G). Most of the Δ*hscA* conidia located in Rab7$^+$ phagosomes were concentrated in the perinuclear region (Figure 4G), where lysosomes accumulate.[41] In p11-KO cells, most of the WT conidia were located in Rab7$^+$ phagosomes at the perinuclear region (Figure 4H). Similar to p11-KO cells, in A549 cells treated with A2ti-1 or p11-KD cells, 75% of the WT and Δ*hscA* conidia were located in Rab7$^+$ phagosomes (Figures 4I and S4F). There were also fewer p47phox$^+$ phagosomes containing WT conidia in A549-Cas9 cells (29%) than in p11-KO cells (41%), and a comparable level of p47phox$^+$ phagosomes containing Δ*hscA* conidia in these cells (Figure 4J).

To investigate whether the HscA-p11-dependent prevention of phagosomal maturation allows for fungal growth inside host cells, we quantified the germination of conidia internalized by A549-Cas9 or p11-KO cells. In general, more dormant conidia and fewer swollen conidia and germlings were found in phagosomes of p11-KO than in A549-Cas9 cells (Figure 4K). The quantification of dormant and swollen conidia showed no significant difference for WT and Δ*hscA* in the same host cells. Hence, deletion of *hscA* does not affect the viability of conidia in the phagosomes at the onset of infection. However, there were more WT (13%) than Δ*hscA* (9%) conidia germinated in phagosomes of A549-Cas9 cells and a similar percentage of 6% of both types of conidia germinated in p11-KO cells (Figure 4K). These results indicate that the failure of phagosomal maturation caused by anchoring of A2t to phagosomes creates a favorable niche for conidia to germinate.

As the aforementioned results were based on immortalized cell lines, we sought to investigate whether the p11-HscA-mediated prevention of phagosomal maturation occurs in primary epithelial cells. We therefore incubated conidia with primary human airway epithelial cells (pAECs). As expected, the p11 on phagosomes containing WT conidia excluded the recruitment of Rab7 to phagosomes (Figures 4L and 4M). There were fewer p11$^+$ phagocytic cups and phagosomes and more Rab7$^+$ phagosomes containing Δ*hscA* conidia than WT conidia in pAEC cells (Figure 4M). This indicates a conserved role of p11 in excluding Rab7 recruitment to phagosomes in epithelial cells.

HscA directs phagosomes to the recycling endosomal pathway and triggers expulsion of conidia

Since p11 plays a role in controlling both the distribution of endosomes containing Rab11—characteristic of recycling endosomes[42]—and exosome release,[43] the expulsion of conidia by cells was analyzed. We observed extracellular conidia stained for p11 (Figure S4B). In contrast to A549 or A549-Cas9 cells (Figures S2B and S3D), we found an accumulation of phagosomes and putative lamellar bodies in the perinuclear region of p11-KO cells (Figures 4H, S3D, and S3E). These observations suggest that *A. fumigatus* manipulates the p11-Rab11 recycling of endosomes to escape phagosomal killing.

Figure 3. HscA anchors the human p11 protein on phagocytic cups and phagosomal membranes

(A and B) LC-MS/MS detection of p11 co-purified with rHscA. (A) Venn diagram showing the number of proteins (in brackets) detected by LC-MS/MS in eluates of 5 different experiments (different colors) with rHscA or in both samples derived from rHscA and rHsp70. (B) Relative abundance of p11 and AnxA2 co-purified with recombinant proteins rHscA and rHsp70. See also Table S1.

(C) HscA-Myc colocalizes with p11 on the surface of A549 cells.

(D) rHscA was not detected on the surface of p11-KO cells after immunostaining.

(E) p11 and AnxA2 are co-purified with HscA-GFP after adding the protein extracts of *hscA-gfp* germlings to A549 cells.

(F and G) p11 is recruited to (F) phagocytic cups (PCs) and (G) PSs of A549 cells. See also Figure S4A.

(H–J) HscA-p11 interaction contributes to adhesion of *A. fumigatus* conidia to host cells. (H) Percentage of p11$^+$ structures (PCs or PSs) containing WT, Δ*hscA*, or Δ*hscA* conidia with rHscA or rHsp70. (I) Number of WT or Δ*hscA* conidia associated with A549-Cas9 or p11-KO cells. (J) Internalization in % of WT or Δ*hscA* conidia by A549-Cas9 or p11-KO cells. For H–J, gray dots represent counting results of individual microscopy images and colored circles represent means of three individual experiments.

(K and L) The level of p11 protein increased after *A. fumigatus* infection. (K) Immunofluorescence staining of A549 cells infected with WT conidia of *A. fumigatus*. Arrows indicate *A. fumigatus* conidia with induced p11$^+$ PCs. "#" marks a cell with low p11 staining intensity. Asterisks indicate p11$^+$ granules. See also Figure S4B. (L) Western blot analysis of p11 and AnxA2 of A549 cells infected with WT conidia at indicated time points. Relative band intensity is indicated. See also Figure S4D.

Statistics: error bars represent the mean ± SD; p values are calculated by paired, two-tailed t test (B) or one-way ANOVA followed by Tukey's multiple comparisons test of the pooled results of individual microscopy images (H–J).

Scale bars, 10 μm.

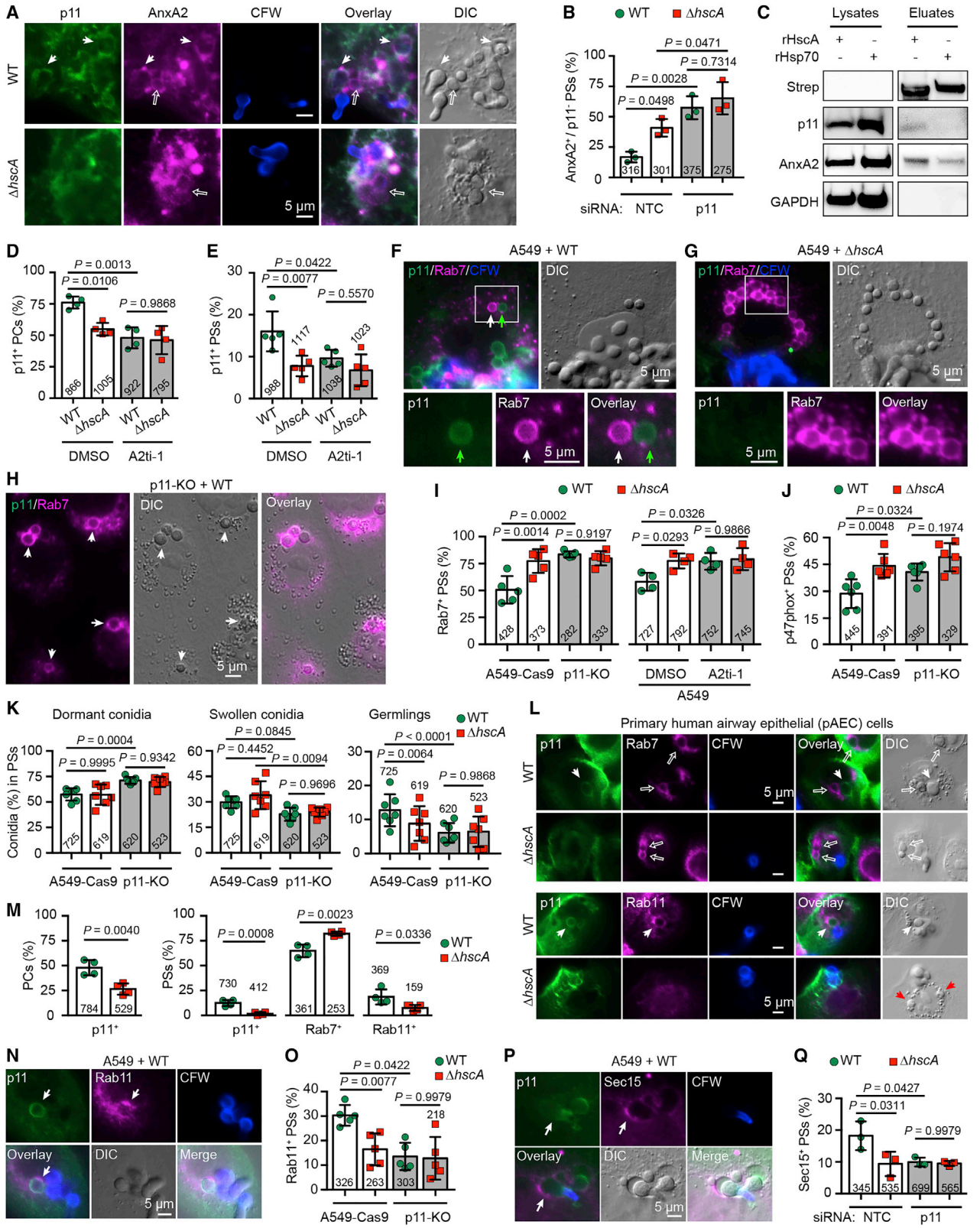

(legend on next page)

To investigate whether Rab11 was recruited to p11$^+$ phagosomes, we stained pAEC and A549 cells infected with conidia for Rab11 that is present on p11$^+$ phagosomes (Figures 4L and 4N). Compared with WT conidia, fewer Δ*hscA* conidia were localized to Rab11-positive (Rab11$^+$) phagosomes of host cells (Figures 4M, 4O, and S4G). Importantly, the proportion of Rab11$^+$ phagosomes was similar for p11-KO or p11-KD cells infected with WT or Δ*hscA* conidia (Figures 4M and S4G), indicating that p11 is essential for HscA-mediated Rab11 recruitment to phagosomes. To substantiate these findings, we analyzed another marker of recycling endosomes and exocytosing vesicles: Sec15, an effector of Rab11.[44] As expected, Sec15 was detected on p11$^+$ phagosomes (Figure 4P) and more WT conidia were localized to Sec15-positive (Sec15$^+$) phagosomes of A549 cells than Δ*hscA* (Figure 4Q). To determine whether this phenotype is caused by HscA, we also incubated A549 cells with rHscA- or rHsp70-coated latex beads. Whereas rHscA-coated beads were found in p11$^+$ phagosomes, rHsp70-coated beads were detected in Rab7$^+$ phagosomes (Figure S5A). Rab11 and Sec15 were also located on p11$^+$ phagosomes containing rHscA beads, but not rHsp70 beads (Figures S5B and S5C). Collectively, these results indicate that WT conidia are more frequently retained in non-matured phagosomes and can thus be delivered to the recycling endosomal pathway.

Since cargo within recycling endosomes is targeted to the cell surface, we hypothesized that conidia are expelled and leave the cell. To test this, we stained A549 cells containing dormant conidia with CFW that exclusively stains conidia outside host cells.[18] Using fluorescence microscopy (Figure 5A), we detected CFW-negative conidia localized to p11$^+$ and Rab11$^+$ phagocytic cup structures (Figure 5B), suggesting these conidia had been redirected to the cell surface. This phenotype is dependent on both HscA and p11. About 2.6% of WT and 0.8% of Δ*hscA* conidia were exocytosed by A549 cells. The percentage for WT conidia was reduced to 1.2% and was unchanged for Δ*hscA* (1%) when incubated with p11-KO cells (Figure 5C). This implies that the interaction of HscA with p11 contributes to the exocytosis of *A. fumigatus* conidia by host cells.

We next sought to substantiate our findings with live-cell imaging. As expected, about 1.3% of WT conidia were exocytosed by A549 cells (Figures 5D and 5E; Video S1), while we did not observe this for Δ*hscA* (Figure 5E). Interestingly, about 1.5% of WT conidia were transferred from a donor cell to a recipient cell (Figures 5F and 5G; Video S2). Again, this was not observed for Δ*hscA* (Figure 5G). These results indicate that targeting of p11 by HscA prevents phagosome maturation, which allows conidia to germinate or to be redirected to the host cell surface.

The rs1873311 SNP in the p11 gene (*S100A10*) decreases the risk of IPA in stem cell transplant recipients

To evaluate our findings in a disease-relevant context, we screened a cohort of hematopoietic stem cell transplant recipients and their corresponding donors for haplotype-tagging single nucleotide polymorphisms (SNPs) in the p11 gene (Figure S6A) and their association with the risk of invasive pulmonary aspergillosis (IPA) (Tables S2 and S3). Among the tag SNPs tested, the donor rs1873311 SNP (T>C) located in the first intron of the p11 gene (Figure 6A) was associated with reduced risk of IPA (Figure 6B; Table S2). In a multivariate model accounting for patient age, sex, and significant clinical variables (Table S3), the T/C genotype contributed to IPA with an adjusted hazard ratio of 0.86 (95% confidence interval, 0.78–0.96: p = 0.026). This indicates a protective effect of the T/C genotype at the rs1873311 locus.

We are aware that, in this particular clinical setting, our proposed mechanism is likely to be mostly relevant in myeloid cells. Therefore, as a proof of concept, we performed experiments in both CD45$^+$ hematopoietic cells isolated from human lung tissue and phagocytes isolated from the blood of healthy donors. Exactly as in epithelial cells, lung CD45$^+$ cells produce p11$^+$ phagosomes and phagocytic cups when confronted with conidia (Figures 6C, 6D, and S7A). More WT (22%) than Δ*hscA* (8%) conidia were consistently detected in p11$^+$ phagosomes (Figures 6E and S7A) and fewer WT (43%) than Δ*hscA* conidia (59%) in Rab7$^+$ phagosomes (Figure 6F) in lung CD45$^+$ cells. Also, rHscA-coated beads were located in p11$^+$ phagosomes, while rHsp70-coated beads were detected in Rab7$^+$ phagosomes (Figure S5D). In neutrophils isolated from blood and containing WT conidia, we also found that p11 excludes Rab7 recruitment to phagosomes (Figure S7B). As shown for macrophages, we detected p11$^+$ and Rab7$^+$ phagosomes containing WT, but not p11$^+$ phagosomes containing Δ*hscA* conidia (Figure S7C). Thus, the presence of

Figure 4. Presence of p11 on phagosomal membrane prevents PS maturation

(A–C) p11 colocalizes with AnxA2 on PSs containing *A. fumigatus* conidia. (A) Immunofluorescence detection of p11 and AnxA2 in A549 cells incubated with conidia. Thin arrows: PSs p11$^+$ and AnxA2$^+$; open arrows: PSs AnxA2$^+$ but p11$^-$. See also Figure S4A. (B) Percentage of AnxA2$^+$/p11$^-$ PSs. NTC, non-targeting control. (C) p11 was precipitated with latex beads coated with rHscA.

(D and E) A2ti-1 inhibits HscA-dependent recruitment of p11 on (D) PCs and (E) PSs.

(F–H) Immunofluorescence analyses of A549 cells infected with (F) WT or (G) Δ*hscA* conidia and (H) p11-KO cells infected with WT conidia. White arrows indicate Rab7$^+$ PSs containing WT conidia. Green arrows mark a p11$^+$ PS containing WT conidia. See also Figure S5A.

(I and J) Percentage of (I) Rab7$^+$ or (J) p47phox$^+$ PSs in A549-Cas9, p11-KO cells, or A549 cells incubated with A2ti-1 or without (only dimethyl sulfoxide, DMSO). See also Figure S4F.

(K) Depletion of p11 reduced germination of *A. fumigatus* conidia inside PSs.

(L) *A. fumigatus* conidia exclude Rab7 recruitment to PSs of pAEC cells by recruiting p11 and Rab11. Thin white arrows indicate p11$^+$ PSs, open arrows mark Rab7$^+$ PSs, thin red arrows indicate internalized Δ*hscA* conidia without p11 or Rab11 staining.

(M) Percentage of p11$^+$ PCs, p11$^+$ PSs, Rab7$^+$ PSs, and Rab11$^+$ PSs containing conidia in pAEC cells.

(N–Q) Recruitment of Rab11 and Sec15 to p11$^+$ PSs. (N and P) Immunofluorescence of (N) p11 and Rab11 or (P) p11 and Sec15 in A549 cells incubated with WT conidia. Arrows indicate PSs with positive staining. See also Figures S5B and S5C. (O and Q) Percentage of (O) Rab11$^+$ or (Q) Sec15$^+$ PSs containing conidia in A549-Cas9 cells, p11-KO cells, or A549 cells treated with non-targeting control or p11-targeting siRNA. See also Figure S4G.

Statistics: error bars represent the mean ± SD; p values calculated by one-way ANOVA (B, D, E, I, J, O, and Q) or repeated measures (RM) one-way ANOVA (K) followed by Tukey's multiple comparisons test or unpaired, two-tailed t test (M).

Scale bars, 5 μm.

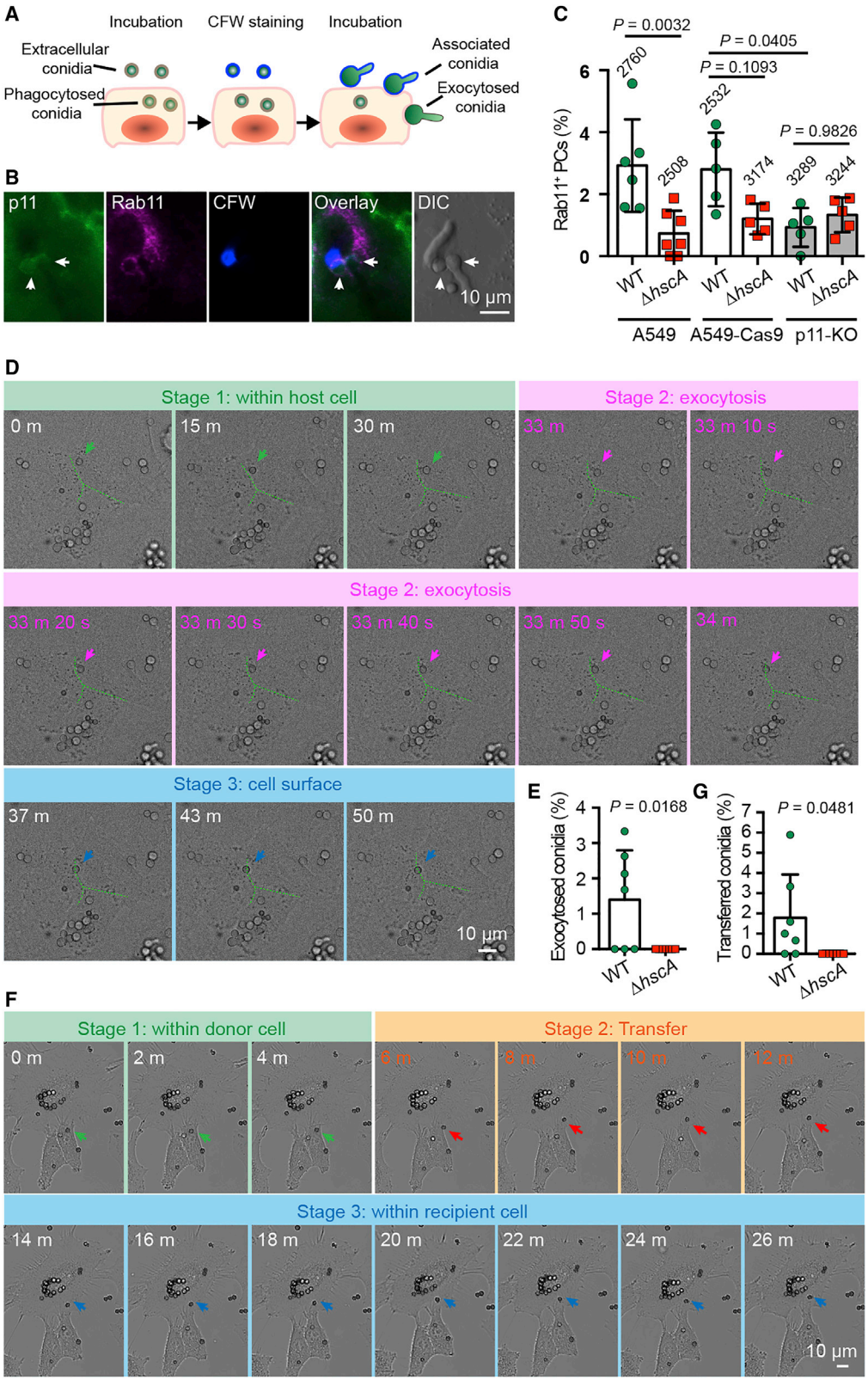

Figure 5. Exocytosis of *A. fumigatus* conidia by host cells

(A) Scheme illustrating the experimental set-up.

(B and C) *A. fumigatus* conidia escape PSs in A549 cells.

(legend continued on next page)

p11 depends on HscA in these phagocytes, indicating that HscA-p11-mediated escape of phagosomal killing is conserved in epithelial cells and phagocytes.

To study the potential function of the rs1873311 SNP in *A. fumigatus* infection, we investigated the DNA sequences of lung epithelial cell lines at the rs1873311 locus. Both the human A549 and pAEC cell lines are T/T homozygous, whereas the human H441 cell line is T/C heterozygous (Figure S6B). We therefore examined the presence of p11 and Rab7 on conidia-containing phagosomes in H441 cells (Figure S7D). A similar percentage of p11$^+$ phagocytic cups (about 40%) or p11$^+$ phagosomes (less than 3%) were observed with both WT and Δ*hscA* conidia (Figure S7E). When we considered Rab7$^+$ phagosomes in H441 cells, slightly fewer WT conidia (71%) than Δ*hscA* conidia (85%) were detected (Figure S7E). Furthermore, the H441 cells had a much higher percentage of Rab7$^+$ phagosomes containing WT conidia than A549 cells (50%) (Figures 2I and 4I). The region containing the SNP rs1873311 in the first intron of p11 is missing in the mouse genome (Figures S6C–E). Therefore, the mouse T7 cell line may represent a cell line lacking a potential regulatory element of p11 encoded in the human SNP region. Indeed, in T7 cells we found a similar percentage for both WT and Δ*hscA* conidia in Rab7$^+$ phagosomes (Figures S7F and S7G).

To substantiate our findings, we generated an A549-T/C isogenic cell line, which has a T/C heterozygous genotype at the rs1873311 locus (Figure S6B). In agreement with our hypothesis, we found fewer p11$^+$ phagocytic cups, p11$^+$ phagosomes, and Rab11$^+$ phagosomes containing WT conidia in A549-T/C cells than in A549-T/T cells. A higher percentage of WT conidia was consistently present in Rab7$^+$ phagosomes of A549-T/C cells compared with A549-T/T cells (Figure 6G). Also, Δ*hscA* conidia induced fewer p11$^+$ phagocytic cups and Rab11$^+$ phagosomes and more Rab7$^+$ phagosomes than WT conidia in the same type of host cells (Figure 6G). Collectively, these results indicate an important functional role of the rs1873311 SNP for maturation of conidia-containing phagosomes.

Since the rs1873311 SNP is not located in the coding region, we hypothesized that it might affect the expression or inducibility of p11 because *A. fumigatus* induced increased p11 levels in A549 cells (Figures 3L and S4B–D). Compared with uninfected cells, an increased p11 signal intensity was observed in A549-T/T and pAEC (T/T) cells but not in A549-T/C, H441 (T/C), or T7 cells (Figures 6H and 6I). We also compared the p11 mRNA levels in cell lines and found increased p11 mRNA levels in A549 and A549-T/T cells after infection, but not in A549-T/C, H441, or T7 cells (Figure 6J). In sum, these results indicate that the rs1873311 SNP affects the expression level of p11 and its inducibility by *A. fumigatus*.

DISCUSSION

The decision whether endosomes enter the degradative or recycling pathway is of fundamental importance for killing of ingested pathogens, and we report the discovery of the human p11 protein as a factor for this decision. The HscA protein present on the conidial surface of *A. fumigatus* acts as a fungal effector protein and anchors p11 on the phagosome, thereby redirecting phagosome development (Figure 7). *A. fumigatus* infection induces increased expression of the human p11 gene and the accumulation of p11 protein, which forms an A2t heterotetramer with AnxA2 at phagocytic cups and phagosomes, independent of the presence of HscA. By binding of conidia to cells, the surface-exposed protein HscA on conidia stabilizes the tetrameric complex on the membrane of phagocytic cups and phagosomes. Anchoring and stabilization of A2t on the phagosomal membrane by HscA directs phagosomes to the secretory pathway by excluding Rab7 but recruiting Rab11 and Sec15 to phagosomes that are markers of recycling endosomes.[42,44] Consequently, our data suggest that conidia escape phagolysosomal killing by (a) germination inside a Rab7-negative phagosome, (b) their lateral transfer to other host cells, or (c) by their release to the extracellular space. When HscA is lacking, p11 dissociates from A2t on the membranes of phagocytic cups and phagosomes. This leads to (d) recruitment of Rab7 to phagosomes and their concentration at the perinuclear region where many lysosomes are located.[41] By fusion of phagosomes with lysosomes, functional phagolysosomes are produced that are characteristic of the degradative pathway leading to killing of conidia (Figure 7).

Fungal and bacterial pathogens have developed various strategies to escape phagolysosomal killing.[45,46] Although A2t and AnxA2 are targeted by viral, bacterial, and fungal pathogens at different stages of infection,[40,47–53] the molecular mechanisms and functional consequences have not been reported before. After infection of *Anxa2*$^{-/-}$ macrophages with *Cryptococcus neoformans*, non-lytic exocytosis decreased, whereas the frequency of lytic exocytosis increased and consequently *Anxa2*$^{-/-}$ mice were more susceptible to *C. neoformans* infection.[49] Given that p11 is rapidly degraded in the absence of AnxA2,[50,54] and based on our results, a role of p11 or A2t in *C. neoformans* non-lytic exocytosis is plausible.

The expression of p11 is induced at the transcriptional and protein level by various stimuli, including cytokines, growth factors, dexamethasone, or the chemotherapy agent paclitaxel.[55,56] With *A. fumigatus* conidia, we discovered another inducer triggering p11 expression. It remains to be shown which molecules of *A. fumigatus* trigger the expression

(B) Immunofluorescence images of potentially exocytosed conidia are indicated by arrows. (C) Percentage of *A. fumigatus* conidia attached to host cells with Rab11$^+$ PCs.

(D–F) Exocytosis and transfer of *A. fumigatus* conidia by A549 cells. (D) Time-lapse image sequence showing exocytosis of WT conidium by A549 cells. See also Video S1. (E) Percentage of exocytosed conidia of indicated strains from A549 cells. (F) Time-lapse image sequence showing transfer of *A. fumigatus* conidium from donor cell to recipient cell. See also Video S2.

(G) Percentage of transfer of conidia of the indicated strains from one A549 cell to another cell.

Data are mean ± SD; p values are for one-way ANOVA followed by Tukey's multiple comparisons test (C) or unpaired, two-tailed t test (E and G).

Scale bars, 10 μm.

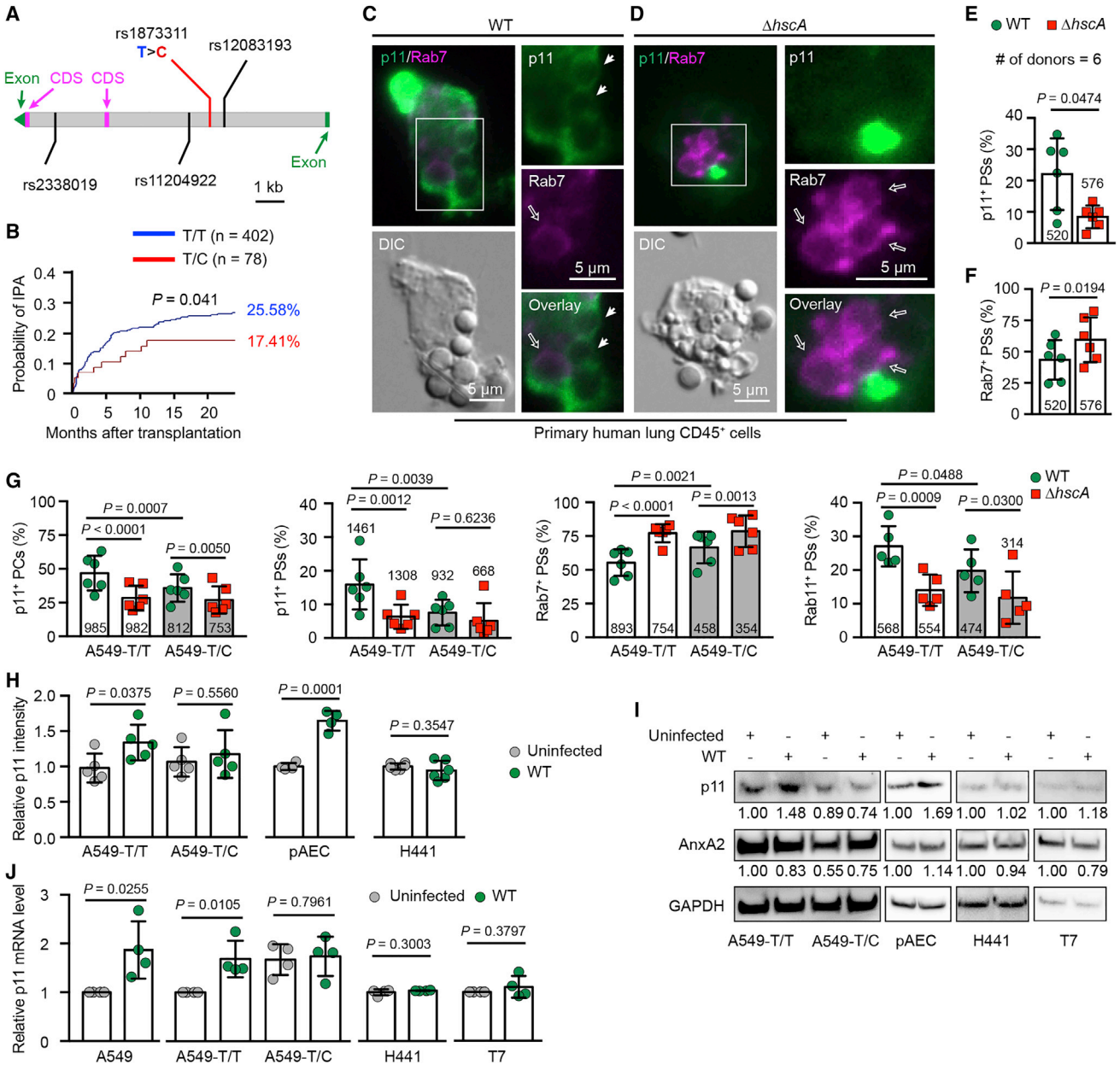

Figure 6. The SNP rs1873311 in the p11 gene interferes with p11 production and decreases the risk of IPA in stem-cell transplant recipients

(A) Position of tag SNPs in human p11 gene. See also Figures S6A–C.

(B) Cumulative incidence of IPA in allogeneic stem-cell transplant recipients according to donor rs1873311 genotypes. *p* value is for Gray's test. See also Tables S2 and S3.

(C–F) p11 excludes recruitment of Rab7 to PSs in primary human lung CD45$^+$ cells. (C and D) CD45$^+$ cells isolated from human lung tissues were infected with (C) WT or (D) Δ*hscA* conidia and were stained for p11 and Rab7. Thin arrows indicate p11$^+$ PSs, open arrows mark Rab7$^+$ PSs. See also Figures S5D and S7A–C. (E and F) Percentage of (E) p11$^+$ PSs and (F) Rab7$^+$ PSs containing conidia in human lung CD45$^+$ cells.

(G–J) *A. fumigatus* infection increases p11 mRNA and protein levels in host cells with T/T, but not with T/C, at the rs1873311 locus. (G) Percentage of p11$^+$ PCs, p11$^+$ PSs, Rab7$^+$ PSs, and Rab11$^+$ PSs containing conidia in A549-T/T or A549-T/C cells. (H) Relative immunofluorescence intensity of p11 in host cells induced by conidia. (I) Western blot analysis of lysates of cells infected with conidia for 4 h. Extracts were probed with the indicated antibodies. (J) Relative p11 mRNA level in indicated cell lines after co-incubation of WT conidia with cells for 4 h.

Statistics: Error bars represent the mean ± SD; p values are calculated by two-tailed t test (paired, E and F; unpaired, H and J) or RM one-way ANOVA followed by Tukey's multiple comparisons test (G).

Scale bars, 5 μm.

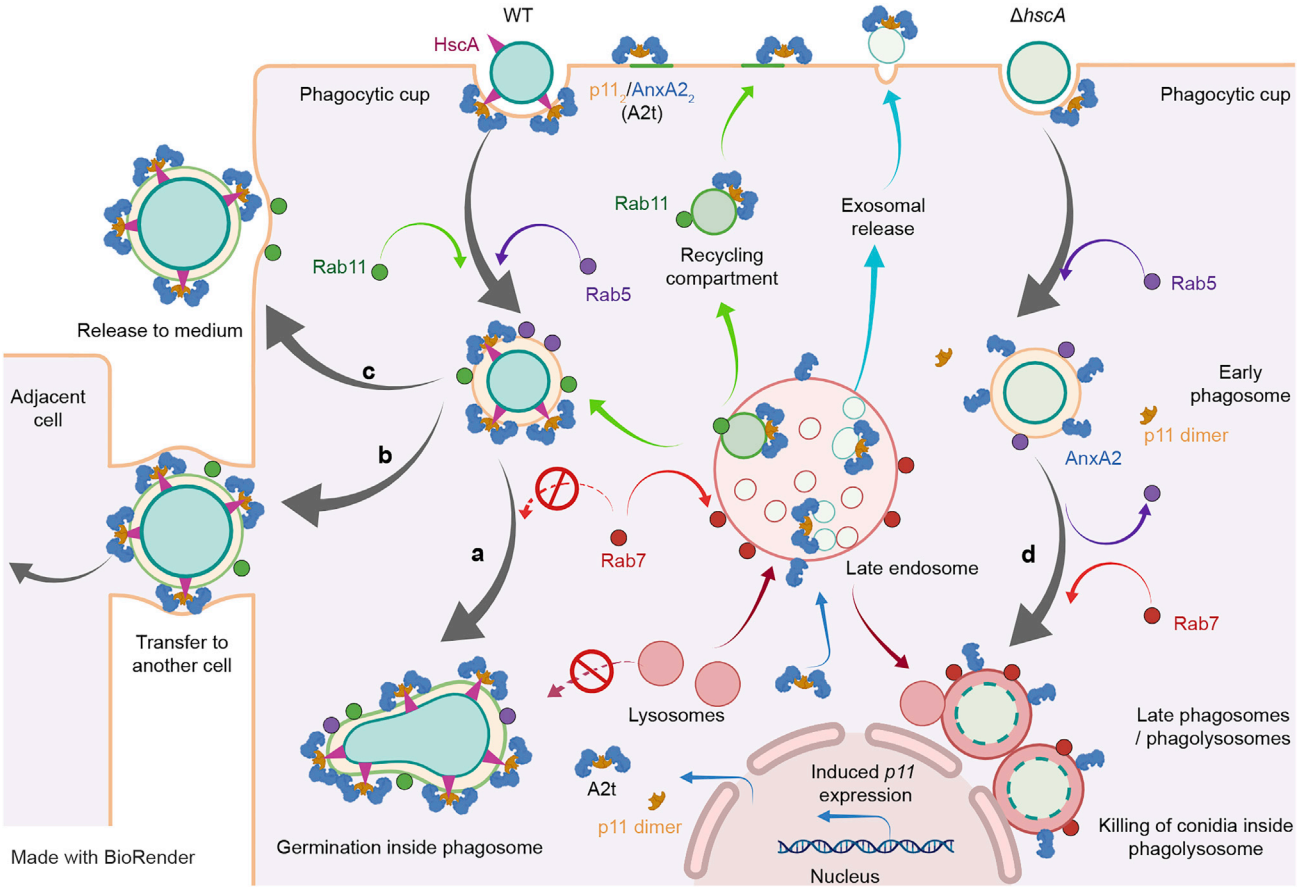

Figure 7. Model of HscA/p11-mediated redirection of PSs to the exocytosis pathway
For details, see text.

of p11 because Δ*hscA* conidia still displayed p11-inducing capacity. For the Δ*hscA* mutant, enrichment of p11 on phagocytic cups was less prominent, likely because anchoring of p11 by HscA was lacking.

As shown here, exocytosis and lateral transfer of conidia are relatively rare events, as similarly observed for the fungal pathogens *C. neoformans* and *Candida albicans*.[57–59] Previously, Shah et al.[60] observed programmed necrosis-dependent lateral transfer of *A. fumigatus*-containing phagosomes from dying human macrophages to other macrophages, suggesting that shuttling was driven by a component derived from the conidial cell wall. Although we cannot exclude that the interaction of HscA with p11 is involved in this process, this seems unlikely because we observed release and transfer of conidia by living cells. In addition, a unidirectional shuttling of conidia initially phagocytosed by neutrophils to macrophages was observed in living zebrafish and mouse phagocytes that involved phagosome transfer.[61] It remains to be shown whether the same shuttling also holds true for human cells. What appears to be comparable is our observation that conidia are also released and transferred by and to A549 cells when still present in phagosomes, since we detected p11 on the surfaces of exocytosed conidia and germlings.

The low expulsion rate we observed raises the question of the clinical relevance of our findings, for which we provided evidence from the analysis of a cohort of patients at risk of IPA. This demonstrated a significant association between an SNP at the p11 locus (rs1873311) and heightened susceptibility to infection. Because there is very low sequence similarity at the SNP locus between the human and mouse p11 gene (Figures S6C–E), the SNP cannot be analyzed in mice. Consequently, it stands to reason that there are likely to be notable differences in function between mouse and human p11. The functional relevance of the SNP was therefore substantiated by comparing the phenotypes of T/T homozygous and T/C heterozygous cells, and the data clearly indicate a regulatory role at the region of the p11 gene covering the SNP.

The association with the donor genome can be explained with identical p11-dependent processing of conidia in epithelial and immune cells. Furthermore, in addition to phagocytes, several studies have highlighted the importance of airway epithelial cells for host defense against invasive aspergillosis.[16,62,63] Therefore, the identified SNP may help to stratify the risk of IPA and identify patients that would benefit the most from antifungal prophylaxis or intensified diagnostics.

STAR★METHODS

Detailed methods are provided in the online version of this paper and include the following:

- KEY RESOURCES TABLE
- RESOURCE AVAILABILITY
  - Lead contact
  - Materials availability
  - Data and code availability
- EXPERIMENTAL MODEL AND SUBJECT DETAILS
  - Cell culture and reagents
  - Fungal strains and cultivation
- METHOD DETAILS
  - Strain construction, Southern and Northern blot analysis
  - Isolation of $CD45^+$ cells from human lung tissues
  - Isolation of PMNs and peripheral blood mononuclear cells from human blood
  - Knockdown and knockout of human p11 gene
  - Gene editing for creating a single-base substitution at the rs1873311 SNP locus
  - Biotinylation of surface proteins
  - Production of antibody against HscA
  - Western blotting
  - Production of purified recombinant HscA and Hsp70
  - Proteomics analysis
  - Infection experiments of cells
  - Immunofluorescence and microscopy
  - Incubation of latex beads with cells
  - RNA isolation, sequencing, and analysis
  - Co-immunoprecipitation
  - Genetic association study
  - SNP selection and genotyping
- QUANTIFICATION AND STATISTICAL ANALYSIS

SUPPLEMENTAL INFORMATION

Supplemental information can be found online at https://doi.org/10.1016/j.chom.2023.02.002.

ACKNOWLEDGMENTS

We thank Silke Steinbach, Sylke Fricke, Natascha Wilker, and Flora Rivieccio for excellent technical assistance and Hendrik Huthoff for critical reading. This work was funded by the Deutsche Forschungsgemeinschaft (DFG) cluster of excellence *Balance of the Microverse* (Project-ID 390713860, Gepris 2051), the DFG-ANR project "AfuInf (316898429)," DFG CRC/Transregio 124 "FungiNet" (A1, Z2; 210879364), DFG CRC 1278 "PolyTarget" (Z01; 316213987), Leibniz project (K217/2016), Fundação para a Ciência e a Tecnologia (FCT) (PTDC/MED-OUT/1112/2021, UIDB/50026/2020, UIDP/50026/2020, NORTE-01-0145-FEDER-000039), EU's Horizon 2020 (847507), "la Caixa" Foundation (ID 100010434) and FCT (LCF/PR/HR17/52190003), Gilead Research Scholars Program - Anti-Fungals, and EU-funded Horizon 2020 project HDM-FUN (ID 847507). M.R. and F.S. were supported by the DFG excellence graduate school Jena School for Microbial Communication, and C.C. by FCT (CEECIND/04058/2018).

AUTHOR CONTRIBUTIONS

Conceptualization, A.A.B., L.J., and O.K.; methodology, L.J., O.K., and A.A.B.; formal analysis, L.J., C.C., A.C., and A.A.B.; investigation, L.J., M.R., L.R., P.H., Z.C., T.K., and F.S.; resources, P.H., T.H., M.S., B.L., T.D., J.F.L., A.C.Jr., and M.T.F.; writing – original draft, L.J., O.K., and A.A.B.; writing – review & editing, L.J. and A.A.B.; visualization, L.J.; supervision, L.J. and A.A.B.; project administration, L.J., O.K., and A.A.B.; funding acquisition, A.A.B., C.C., and A.C.

DECLARATION OF INTERESTS

The authors declare no competing interests.

INCLUSION AND DIVERSITY

We worked to ensure gender balance in the recruitment of human subjects.

Received: July 8, 2022
Revised: November 28, 2022
Accepted: February 3, 2023
Published: March 8, 2023

REFERENCES

1. Cullen, P.J., and Steinberg, F. (2018). To degrade or not to degrade: mechanisms and significance of endocytic recycling. Nat. Rev. Mol. Cell Biol. *19*, 679–696. https://doi.org/10.1038/s41580-018-0053-7.
2. Brakhage, A.A., Zimmermann, A.-K., Rivieccio, F., Visser, C., and Blango, M.G. (2021). Host-derived extracellular vesicles for antimicrobial defense. microLife *2*. uqab003. https://doi.org/10.1093/femsml/uqab003.
3. Kinchen, J.M., and Ravichandran, K.S. (2008). Phagosome maturation: going through the acid test. Nat. Rev. Mol. Cell Biol. *9*, 781–795. https://doi.org/10.1038/nrm2515.
4. Serra, N.D., and Sundaram, M.V. (2021). Transcytosis in the development and morphogenesis of epithelial tissues. EMBO J. *40*, e106163. https://doi.org/10.15252/embj.2020106163.
5. Yarwood, R., Hellicar, J., Woodman, P.G., and Lowe, M. (2020). Membrane trafficking in health and disease. Dis. Model. Mech. *13*, dmm043448. https://doi.org/10.1242/dmm.043448.
6. Xie, J., Zhang, P., Crite, M., Lindsay, C.V., and DiMaio, D. (2021). Retromer stabilizes transient membrane insertion of L2 capsid protein during retrograde entry of human papillomavirus. Sci. Adv. *7*, eabh4276. https://doi.org/10.1126/sciadv.abh4276.
7. Walpole, G.F.W., Plumb, J.D., Chung, D., Tang, B., Boulay, B., Osborne, D.G., Piotrowski, J.T., Catz, S.D., Billadeau, D.D., Grinstein, S., and Jaumouillé, V. (2020). Inactivation of Rho GTPases by *Burkholderia cenocepacia* induces a WASH-mediated actin polymerization that delays phagosome maturation. Cell Rep. *31*, 107721. https://doi.org/10.1016/j.celrep.2020.107721.
8. Ledvina, H.E., Kelly, K.A., Eshraghi, A., Plemel, R.L., Peterson, S.B., Lee, B., Steele, S., Adler, M., Kawula, T.H., Merz, A.J., et al. (2018). A phosphatidylinositol 3-kinase effector alters phagosomal maturation to promote intracellular growth of *Francisella*. Cell Host Microbe *24*, 285–295.e8. https://doi.org/10.1016/j.chom.2018.07.003.
9. Schmidt, F., Thywißen, A., Goldmann, M., Cunha, C., Cseresnyés, Z., Schmidt, H., Rafiq, M., Galiani, S., Gräler, M.H., Chamilos, G., et al. (2020). Flotillin-dependent membrane microdomains are required for functional phagolysosomes against fungal infections. Cell Rep. *32*, 108017. https://doi.org/10.1016/j.celrep.2020.108017.
10. Wei, D., Zhan, W., Gao, Y., Huang, L., Gong, R., Wang, W., Zhang, R., Wu, Y., Gao, S., and Kang, T. (2021). RAB31 marks and controls an ESCRT-independent exosome pathway. Cell Res. *31*, 157–177. https://doi.org/10.1038/s41422-020-00409-1.
11. van Niel, G., D'Angelo, G., and Raposo, G. (2018). Shedding light on the cell biology of extracellular vesicles. Nat. Rev. Mol. Cell Biol. *19*, 213–228. https://doi.org/10.1038/nrm.2017.125.
12. Dagenais, T.R.T., and Keller, N.P. (2009). Pathogenesis of *Aspergillus fumigatus* in invasive Aspergillosis. Clin. Microbiol. Rev. *22*, 447–465. https://doi.org/10.1128/CMR.00055-08.

13. Latgé, J.P., and Chamilos, G. (2019). *Aspergillus fumigatus* and Aspergillosis in 2019. Clin. Microbiol. Rev. *33*, e00140-18–e00118. https://doi.org/10.1128/CMR.00140-18.

14. Brakhage, A.A. (2005). Systemic fungal infections caused by *Aspergillus* species: epidemiology, infection process and virulence determinants. Curr. Drug Targets *6*, 875–886. https://doi.org/10.2174/138945005774912717.

15. Taccone, F.S., Van den Abeele, A.-M., Bulpa, P., Misset, B., Meersseman, W., Cardoso, T., Paiva, J.-A., Blasco-Navalpotro, M., De Laere, E., Dimopoulos, G., et al. (2015). Epidemiology of invasive aspergillosis in critically ill patients: clinical presentation, underlying conditions, and outcomes. Crit. Care *19*, 7. https://doi.org/10.1186/s13054-014-0722-7.

16. Amin, S., Thywissen, A., Heinekamp, T., Saluz, H.P., and Brakhage, A.A. (2014). Melanin dependent survival of *Apergillus fumigatus* conidia in lung epithelial cells. Int. J. Med. Microbiol. *304*, 626–636. https://doi.org/10.1016/j.ijmm.2014.04.009.

17. Seidel, C., Moreno-Velásquez, S.D., Ben-Ghazzi, N., Gago, S., Read, N.D., and Bowyer, P. (2020). Phagolysosomal survival enables non-lytic hyphal escape and ramification through lung epithelium during *Aspergillus fumigatus* infection. Front. Microbiol. *11*, 1955. https://doi.org/10.3389/fmicb.2020.01955.

18. Thywißen, A., Heinekamp, T., Dahse, H.-M., Schmaler-Ripcke, J., Nietzsche, S., Zipfel, P.F., and Brakhage, A.A. (2011). Conidial dihydroxynaphthalene melanin of the human pathogenic fungus *Aspergillus fumigatus* interferes with the host endocytosis pathway. Front. Microbiol. *2*, 96. https://doi.org/10.3389/fmicb.2011.00096.

19. Jahn, B., Langfelder, K., Schneider, U., Schindel, C., and Brakhage, A.A. (2002). PKSP-dependent reduction of phagolysosome fusion and intracellular kill of *Aspergillus fumigatus* conidia by human monocyte-derived macrophages. Cell Microbiol. *4*, 793–803. https://doi.org/10.1046/j.1462-5822.2002.00228.x.

20. Flannagan, R.S., Jaumouillé, V., and Grinstein, S. (2012). The cell biology of phagocytosis. Annu. Rev. Pathol. *7*, 61–98. https://doi.org/10.1146/annurev-pathol-011811-132445.

21. Erwig, L.P., and Gow, N.A.R. (2016). Interactions of fungal pathogens with phagocytes. Nat. Rev. Microbiol. *14*, 163–176. https://doi.org/10.1038/nrmicro.2015.21.

22. Kyrmizi, I., Ferreira, H., Carvalho, A., Figueroa, J.A.L., Zarmpas, P., Cunha, C., Akoumianaki, T., Stylianou, K., Deepe, G.S., Jr., Samonis, G., et al. (2018). Calcium sequestration by fungal melanin inhibits calcium-calmodulin signalling to prevent LC3-associated phagocytosis. Nat. Microbiol. *3*, 791–803. https://doi.org/10.1038/s41564-018-0167-x.

23. Akoumianaki, T., Kyrmizi, I., Valsecchi, I., Gresnigt, M.S., Samonis, G., Drakos, E., Boumpas, D., Muszkieta, L., Prevost, M.C., Kontoyiannis, D.P., et al. (2016). *Aspergillus* cell wall melanin blocks LC3-associated phagocytosis to promote pathogenicity. Cell Host Microbe *19*, 79–90. https://doi.org/10.1016/j.chom.2015.12.002.

24. Jia, L.-J., Krüger, T., Blango, M.G., von Eggeling, F., Kniemeyer, O., and Brakhage, A.A. (2020). Biotinylated surfome profiling identifies potential biomarkers for diagnosis and therapy of *Aspergillus fumigatus* infection. mSphere *5*, e00535-20–e00520. https://doi.org/10.1128/mSphere.00535-20.

25. Liu, H., Lee, M.J., Solis, N.V., Phan, Q.T., Swidergall, M., Ralph, B., Ibrahim, A.S., Sheppard, D.C., and Filler, S.G. (2016). *Aspergillus fumigatus* CalA binds to integrin $\alpha5\beta1$ and mediates host cell invasion. Nat. Microbiol. *2*, 16211. https://doi.org/10.1038/nmicrobiol.2016.211.

26. Voltersen, V., Blango, M.G., Herrmann, S., Schmidt, F., Heinekamp, T., Strassburger, M., Krüger, T., Bacher, P., Lother, J., Weiss, E., et al. (2018). Proteome analysis reveals the conidial surface protein CcpA essential for virulence of the pathogenic fungus *Aspergillus fumigatus*. mBio *9*, e01557-18–e01518. https://doi.org/10.1128/mBio.01557-18.

27. Wasylnka, J.A., and Moore, M.M. (2003). *Aspergillus fumigatus* conidia survive and germinate in acidic organelles of A549 epithelial cells. J. Cell Sci. *116*, 1579–1587. https://doi.org/10.1242/jcs.00329.

28. Rink, J., Ghigo, E., Kalaidzidis, Y., and Zerial, M. (2005). Rab conversion as a mechanism of progression from early to late endosomes. Cell *122*, 735–749. https://doi.org/10.1016/j.cell.2005.06.043.

29. Bucci, C., Thomsen, P., Nicoziani, P., McCarthy, J., van Deurs, B., and Pfeffer, S.R. (2000). Rab7: a key to lysosome biogenesis. Mol. Biol. Cell *11*, 467–480. https://doi.org/10.1091/mbc.11.2.467.

30. Vieira, O.V., Bucci, C., Harrison, R.E., Trimble, W.S., Lanzetti, L., Gruenberg, J., Schreiber, A.D., Stahl, P.D., and Grinstein, S. (2003). Modulation of Rab5 and Rab7 recruitment to phagosomes by phosphatidylinositol 3-kinase. Mol. Cell Biol. *23*, 2501–2514. https://doi.org/10.1128/mcb.23.7.2501-2514.2003.

31. Gerke, V., and Weber, K. (1984). Identity of p36K phosphorylated upon Rous sarcoma virus transformation with a protein purified from brush borders; calcium-dependent binding to non-erythroid spectrin and F-actin. EMBO J. *3*, 227–233. https://doi.org/10.1002/j.1460-2075.1984.tb01789.x.

32. He, K.L., Deora, A.B., Xiong, H., Ling, Q., Weksler, B.B., Niesvizky, R., and Hajjar, K.A. (2008). Endothelial cell annexin A2 regulates polyubiquitination and degradation of its binding partner S100A10/p11. J. Biol. Chem. *283*, 19192–19200. https://doi.org/10.1074/jbc.M800100200.

33. Deora, A.B., Kreitzer, G., Jacovina, A.T., and Hajjar, K.A. (2004). An annexin 2 phosphorylation switch mediates p11-dependent translocation of annexin 2 to the cell surface. J. Biol. Chem. *279*, 43411–43418. https://doi.org/10.1074/jbc.M408078200.

34. Fang, Y.-T., Lin, C.-F., Wang, C.-Y., Anderson, R., and Lin, Y.-S. (2012). Interferon-γ stimulates p11-dependent surface expression of annexin A2 in lung epithelial cells to enhance phagocytosis. J. Cell. Physiol. *227*, 2775–2787. https://doi.org/10.1002/jcp.23026.

35. Emans, N., Gorvel, J.P., Walter, C., Gerke, V., Kellner, R., Griffiths, G., and Gruenberg, J. (1993). Annexin II is a major component of fusogenic endosomal vesicles. J. Cell Biol. *120*, 1357–1369. https://doi.org/10.1083/jcb.120.6.1357.

36. Morel, E., Parton, R.G., and Gruenberg, J. (2009). Annexin A2-dependent polymerization of actin mediates endosome biogenesis. Dev. Cell *16*, 445–457. https://doi.org/10.1016/j.devcel.2009.01.007.

37. Morel, E., and Gruenberg, J. (2007). The p11/S100A10 light chain of annexin A2 is dispensable for annexin A2 association to endosomes and functions in endosomal transport. PLoS One *2*, e1118. https://doi.org/10.1371/journal.pone.0001118.

38. Goldmann, M., Schmidt, F., Kyrmizi, I., Chamilos, G., and Brakhage, A.A. (2021). Isolation and immunofluorescence staining of *Aspergillus fumigatus* conidia-containing phagolysosomes. STAR Protoc. *2*, 100328. https://doi.org/10.1016/j.xpro.2021.100328.

39. Reddy, T.R.K., Li, C., Fischer, P.M., and Dekker, L.V. (2012). Three-dimensional pharmacophore design and biochemical screening identifies substituted 1,2,4-triazoles as inhibitors of the Annexin A2-S100A10 protein interaction. ChemMedChem *7*, 1435–1446. https://doi.org/10.1002/cmdc.201200107.

40. Woodham, A.W., Taylor, J.R., Jimenez, A.I., Skeate, J.G., Schmidt, T., Brand, H.E., Da Silva, D.M., and Kast, W.M. (2015). Small molecule inhibitors of the annexin A2 heterotetramer prevent human papillomavirus type 16 infection. J. Antimicrob. Chemother. *70*, 1686–1690. https://doi.org/10.1093/jac/dkv045.

41. Korolchuk, V.I., Saiki, S., Lichtenberg, M., Siddiqi, F.H., Roberts, E.A., Imarisio, S., Jahreiss, L., Sarkar, S., Futter, M., Menzies, F.M., et al. (2011). Lysosomal positioning coordinates cellular nutrient responses. Nat. Cell Biol. *13*, 453–460. https://doi.org/10.1038/ncb2204.

42. Zobiack, N., Rescher, U., Ludwig, C., Zeuschner, D., and Gerke, V. (2003). The Annexin 2/S100A10 complex controls the distribution of transferrin receptor-containing recycling endosomes. Mol. Biol. Cell *14*, 4896–4908. https://doi.org/10.1091/mbc.e03-06-0387.

43. Chen, Y.-D., Fang, Y.-T., Cheng, Y.-L., Lin, C.-F., Hsu, L.-J., Wang, S.-Y., Anderson, R., Chang, C.-P., and Lin, Y.-S. (2017). Exophagy of annexin A2 via RAB11, RAB8A and RAB27A in IFN-γ-stimulated lung epithelial cells. Sci. Rep. *7*, 5676. https://doi.org/10.1038/s41598-017-06076-4.

44. Zhang, X.-M., Ellis, S., Sriratana, A., Mitchell, C.A., and Rowe, T. (2004). Sec15 is an effector for the Rab11 GTPase in mammalian cells. J. Biol. Chem. *279*, 43027–43034. https://doi.org/10.1074/jbc.M402264200.

45. Pauwels, A.-M., Trost, M., Beyaert, R., and Hoffmann, E. (2017). Patterns, receptors, and signals: regulation of phagosome maturation. Trends Immunol. *38*, 407–422. https://doi.org/10.1016/j.it.2017.03.006.

46. Westman, J., Walpole, G.F.W., Kasper, L., Xue, B.Y., Elshafee, O., Hube, B., and Grinstein, S. (2020). Lysosome fusion maintains phagosome integrity during fungal infection. Cell Host Microbe *28*, 798–812.e6. https://doi.org/10.1016/j.chom.2020.09.004.

47. Jolly, C., Winfree, S., Hansen, B., and Steele-Mortimer, O. (2014). The Annexin A2/p11 complex is required for efficient invasion of *Salmonella* Typhimurium in epithelial cells. Cell Microbiol. *16*, 64–77. https://doi.org/10.1111/cmi.12180.

48. Li, R., Tan, S., Yu, M., Jundt, M.C., Zhang, S., and Wu, M. (2015). Annexin A2 regulates autophagy in *Pseudomonas aeruginosa* infection through the Akt1-mTOR-ULK1/2 signaling pathway. J. Immunol. *195*, 3901–3911. https://doi.org/10.4049/jimmunol.1500967.

49. Stukes, S., Coelho, C., Rivera, J., Jedlicka, A.E., Hajjar, K.A., and Casadevall, A. (2016). The membrane phospholipid binding protein Annexin A2 promotes phagocytosis and nonlytic exocytosis of *Cryptococcus neoformans* and impacts survival in fungal infection. J. Immunol. *197*, 1252–1261. https://doi.org/10.4049/jimmunol.1501855.

50. Taylor, J.R., Fernandez, D.J., Thornton, S.M., Skeate, J.G., Lühen, K.P., Da Silva, D.M., Langen, R., and Kast, W.M. (2018). Heterotetrameric annexin A2/S100A10 (A2t) is essential for oncogenic human papillomavirus trafficking and capsid disassembly, and protects virions from lysosomal degradation. Sci. Rep. *8*, 11642. https://doi.org/10.1038/s41598-018-30051-2.

51. Dziduszko, A., and Ozbun, M.A. (2013). Annexin A2 and S100A10 regulate human papillomavirus type 16 entry and intracellular trafficking in human keratinocytes. J. Virol. *87*, 7502–7515. https://doi.org/10.1128/JVI.00519-13.

52. Taylor, J.R., Skeate, J.G., and Kast, W.M. (2018). Annexin A2 in virus infection. Front. Microbiol. *9*, 2954. https://doi.org/10.3389/fmicb.2018.02954.

53. He, S., Li, X., Li, R., Fang, L., Sun, L., Wang, Y., and Wu, M. (2016). Annexin A2 Modulates ROS and Impacts Inflammatory Response via IL-17 Signaling in Polymicrobial Sepsis Mice. PLoS Pathog. *12*, e1005743. https://doi.org/10.1371/journal.ppat.1005743.

54. Puisieux, A., Ji, J., and Ozturk, M. (1996). Annexin II up-regulates cellular levels of p11 protein by a post-translational mechanisms. Biochem. J. *313*, 51–55. (Pt 1). https://doi.org/10.1042/bj3130051.

55. Svenningsson, P., and Greengard, P. (2007). p11 (S100A10) — an inducible adaptor protein that modulates neuronal functions. Curr. Opin. Pharmacol. *7*, 27–32. https://doi.org/10.1016/j.coph.2006.10.001.

56. Lu, H., Xie, Y., Tran, L., Lan, J., Yang, Y., Murugan, N.L., Wang, R., Wang, Y.J., and Semenza, G.L. (2020). Chemotherapy-induced S100A10 recruits KDM6A to facilitate OCT4-mediated breast cancer stemness. J. Clin. Invest. *130*, 4607–4623. https://doi.org/10.1172/JCI138577.

57. Bain, J.M., Lewis, L.E., Okai, B., Quinn, J., Gow, N.A.R., and Erwig, L.-P. (2012). Non-lytic expulsion/exocytosis of *Candida albicans* from macrophages. Fungal Genet. Biol. *49*, 677–678. https://doi.org/10.1016/j.fgb.2012.01.008.

58. Ma, H., Croudace, J.E., Lammas, D.A., and May, R.C. (2006). Expulsion of live pathogenic yeast by macrophages. Curr. Biol. *16*, 2156–2160. https://doi.org/10.1016/j.cub.2006.09.032.

59. Ma, H., Croudace, J.E., Lammas, D.A., and May, R.C. (2007). Direct cell-to-cell spread of a pathogenic yeast. BMC Immunol. *8*, 15. https://doi.org/10.1186/1471-2172-8-15.

60. Shah, A., Kannambath, S., Herbst, S., Rogers, A., Soresi, S., Carby, M., Reed, A., Mostowy, S., Fisher, M.C., Shaunak, S., and Armstrong-James, D.P. (2016). Calcineurin orchestrates lateral transfer of *Aspergillus fumigatus* during macrophage cell death. Am. J. Respir. Crit. Care Med. *194*, 1127–1139. https://doi.org/10.1164/rccm.201601-0070OC.

61. Pazhakh, V., Ellett, F., Croker, B.A., O'Donnell, J.A., Pase, L., Schulze, K.E., Greulich, R.S., Gupta, A., Reyes-Aldasoro, C.C., Andrianopoulos, A., and Lieschke, G.J. (2019). β-glucan–dependent shuttling of conidia from neutrophils to macrophages occurs during fungal infection establishment. PLoS Biol. *17*, e3000113. https://doi.org/10.1371/journal.pbio.3000113.

62. Ewald, J., Rivieccio, F., Radosa, L., Schuster, S., Brakhage, A.A., and Kaleta, C. (2021). Dynamic optimization reveals alveolar epithelial cells as key mediators of host defense in invasive aspergillosis. PLoS Comput. Biol. *17*, e1009645. https://doi.org/10.1371/journal.pcbi.1009645.

63. Bertuzzi, M., Howell, G.J., Thomson, D.D., Fortune-Grant, R., Möslinger, A., Dancer, P., Van Rhijn, N., Motsi, N., Du, X., Codling, A., et al. (2022). Epithelial uptake of *Aspergillus fumigatus* drives efficient fungal clearance *in vivo* and is aberrant in Chronic Obstructive Pulmonary Disease (COPD). Preprint at bioRxiv. https://doi.org/10.1101/2022.02.01.478664.

64. Perez-Riverol, Y., Bai, J., Bandla, C., García-Seisdedos, D., Hewapathirana, S., Kamatchinathan, S., Kundu, D.J., Prakash, A., Frericks-Zipper, A., Eisenacher, M., et al. (2022). The PRIDE database resources in 2022: a hub for mass spectrometry-based proteomics evidences. Nucleic Acids Res. *50*, D543–D552. https://doi.org/10.1093/nar/gkab1038.

65. da Silva Ferreira, M.E., Kress, M.R.V.Z., Savoldi, M., Goldman, M.H.S., Härtl, A., Heinekamp, T., Brakhage, A.A., and Goldman, G.H. (2006). The *akuB*(KU80) mutant deficient for nonhomologous end joining is a powerful tool for analyzing pathogenicity in *Aspergillus fumigatus*. Eukaryot. Cell *5*, 207–211. https://doi.org/10.1128/EC.5.1.207-211.2006.

66. Lapp, K., Vödisch, M., Kroll, K., Strassburger, M., Kniemeyer, O., Heinekamp, T., and Brakhage, A.A. (2014). Characterization of the *Aspergillus fumigatus* detoxification systems for reactive nitrogen intermediates and their impact on virulence. Front. Microbiol. *5*, 469. https://doi.org/10.3389/fmicb.2014.00469.

67. Valiante, V., Baldin, C., Hortschansky, P., Jain, R., Thywißen, A., Straßburger, M., Shelest, E., Heinekamp, T., and Brakhage, A.A. (2016). The *Aspergillus fumigatus* conidial melanin production is regulated by the bifunctional bHLH DevR and MADS-box RlmA transcription factors. Mol. Microbiol. *102*, 321–335. https://doi.org/10.1111/mmi.13462.

68. Gao, P., Dong, X., Wang, Y., and Wei, G.H. (2021). Optimized CRISPR/Cas9-mediated single nucleotide mutation in adherent cancer cell lines. STAR Protoc. *2*, 100419. https://doi.org/10.1016/j.xpro.2021.100419.

69. Ran, F.A., Hsu, P.D., Wright, J., Agarwala, V., Scott, D.A., and Zhang, F. (2013). Genome engineering using the CRISPR-Cas9 system. Nat. Protoc. *8*, 2281–2308. https://doi.org/10.1038/nprot.2013.143.

70. Dersch, P., and Isberg, R.R. (1999). A region of the *Yersinia pseudotuberculosis* invasin protein enhances integrin-mediated uptake into mammalian cells and promotes self-association. EMBO J. *18*, 1199–1213. https://doi.org/10.1093/emboj/18.5.1199.

71. De Pauw, B., Walsh, T.J., Donnelly, J.P., Stevens, D.A., Edwards, J.E., Calandra, T., Pappas, P.G., Maertens, J., Lortholary, O., Kauffman, C.A., et al. (2008). Revised definitions of invasive fungal disease from the European Organization for Research and Treatment of Cancer/Invasive Fungal Infections Cooperative Group and the National Institute of Allergy and Infectious Diseases Mycoses Study Group (EORTC/MSG) Consensus Group. Clin. Infect. Dis. *46*, 1813–1821. https://doi.org/10.1086/588660.

72. Gray, R.J. (1988). A Class of *K*-Sample Tests for Comparing the Cumulative Incidence of a Competing Risk. Ann. Statist. *16*. https://doi.org/10.1214/aos/1176350951.

73. Scrucca, L., Santucci, A., and Aversa, F. (2007). Competing risk analysis using R: an easy guide for clinicians. Bone Marrow Transplant. *40*, 381–387. https://doi.org/10.1038/sj.bmt.1705727.

74. Scrucca, L., Santucci, A., and Aversa, F. (2010). Regression modeling of competing risk using R: an in depth guide for clinicians. Bone Marrow Transplant. *45*, 1388–1395. https://doi.org/10.1038/bmt.2009.359.

STAR★METHODS

KEY RESOURCES TABLE

REAGENT or RESOURCE	SOURCE	IDENTIFIER
Antibodies		
CD45 Antibody, anti-human, Biotin, REAfinity™	Miltenyi Biotec	Cat# 130-110-768; RRID: AB_2658256
Goat polyclonal anti-mouse IgG (H + L), Alexa Fluor 488	Thermo Fisher Scientific	Cat# A-11029; RRID: AB_2534088
Goat polyclonal anti-mouse IgG (H + L), DyLight 633	Thermo Fisher Scientific	Cat# 35512; RRID: AB_1307538
Goat polyclonal anti-rabbit IgG (H + L), DyLight 633	Thermo Fisher Scientific	Cat# 35562; RRID: AB_1307539
Goat polyclonal anti-rabbit IgG (H&L), HRP conjugated	Abcam	Cat# Ab6721; RRID: AB_955447
Horse polyclonal anti-mouse IgG, HRP-linked antibody	Cell Signaling Technology	Cat# 7076; RRID: AB_330924
Mouse monoclonal anti-biotin	Thermo Fisher Scientific	Cat# MA5-11251; RRID: AB_10980856
Mouse monoclonal anti-GAPDH	Proteintech	Cat# 60004-1-Ig; RRID: AB_2107436
Mouse monoclonal anti-GFP	Santa Cruz	Cat# sc-9996; RRID: AB_627695
Mouse monoclonal anti-Hsp70	Thermo Fisher Scientific	Cat# MA3-006; RRID: AB_325454
Mouse monoclonal anti-Myc-Tag	Cell Signaling Technology	Cat# 2276S; RRID: AB_331783
Mouse monoclonal anti-p11	BD	Cat# 610071; RRID: AB_397482
Mouse monoclonal anti-p36	BD	Cat# 610068; RRID: AB_397480
Mouse monoclonal StrepMAB-Classic	IBA Lifesciences	Cat# 2-1507-001
Rabbit monoclonal anti-Annexin A2	Cell Signaling Technology	Cat# 8235; RRID: AB_11129437
Rabbit monoclonal anti-Rab7	Cell Signaling Technology	Cat# 9367; RRID: AB_1904103
Rabbit monoclonal anti-β-actin	Cell Signaling Technology	Cat# 8457; RRID: AB_10950489
Rabbit polyclonal anti-GFP	Abcam	Cat# Ab290; RRID: AB_303395
Rabbit polyclonal anti-Myc	Abcam	Cat# Ab9106; RRID: AB_307014
Rabbit polyclonal anti-HscA	This paper	N/A
Rabbit polyclonal anti-p47phox	Santa Cruz Biotechnology	Cat# sc-14015; RRID: AB_2150289
Rabbit polyclonal anti-Rab11a	Cell Signaling Technology	Cat# 2413; RRID: AB_2173452
Rabbit polyclonal anti-Sec15	Thermo Fisher Scientific	Cat# PA5-66234; RRID: AB_2664154
Sheep Anti-Digoxigenin Fab fragments Antibody	Roche	Cat# 11093274910; RRID: AB_514497
Bacterial and virus strains		
E. coli BL21 (DE3)	New England Biolabs	Cat# C2527
E. coli NEB Turbo Competent (High Efficiency)	New England Biolabs	Cat# C2984
Biological samples		
Human lung tissues	Jena University Hospital	N/A
Buffy coats	Jena University Hospital	N/A
Chemicals, peptides, and recombinant proteins		
A2ti-1	MedChemExpress	Cat# HY-136465
BSA (used for beads coating)	AppliChem	Cat# A1391
BSA (used for cell culture)	Sigma-Aldrich	Cat# A9418
Calcofluor white	Sigma-Aldrich	Cat# 18909
Congo red	Sigma-Aldrich	Cat# C6277
cOmplete™, Mini, EDTA-free Protease Inhibitor Cocktail	Roche	Cat# 04693159001
DNase I from bovine pancreas	Sigma-Aldrich	Cat# DN25
DharmaFECT 1 Transfection Reagent	Horizon Discovery	Cat# T-2001-02
DIG-11-dUTP	Jena Bioscience	Cat# NU-803-DIGXS
Dispase (from *Bacillus polymyxa*)	Corning	Cat# 734-1312
DNase I from bovine pancreas	Roche	Cat# 11284932001
DSP	Thermo Fisher Scientific	Cat# 22585

(*Continued on next page*)

Continued

REAGENT or RESOURCE	SOURCE	IDENTIFIER
Elastase from porcine pancreas	Sigma-Aldrich	Cat# E7885
EZ-Link Sulfo-NHS-LC-Biotin	Thermo Fisher Scientific	Cat# 21335
Fibronectin	Sigma-Aldrich	Cat# F1141
Hygromycin B	InvivoGen	Cat# ant-hg-1
Insulin-Transferrin-Selenium	Thermo Fisher Scientific	Cat# 41400045
iTaq™ Universal SYBR® Green Supermix	Bio-Rad	Cat# 1725122
LysoTracker red DND-99	Thermo Fisher Scientific	Cat# L7528
Recombinant human IFN-γ	Gibco	Cat# PHC4031
rHscA	This paper	N/A
rHsp70	This paper	N/A
Streptavidin, Alexa Fluor ™ 488 conjugate	Thermo Fisher Scientific	Cat# S11223
Trypsin/Lys-C mixture, Mass Spec Grade	Promega	Cat# V5071
TrypLE™ Express	Gibco	Cat# 12604-013
Tunicamycin	Sigma-Aldrich	Cat# T7765
Wheat Germ agglutinin, Oregon Green ™ 488 Conjugate	Thermo Fisher Scientific	Cat# W6748
Critical commercial assays		
CyQUANT™ LDH Cytotoxicity Assay	Thermo Fisher Scientific	Cat# C20300
LEGENDScreen™ Human PE Kit	BioLegend	Cat# 700007
Maxima H Minus First Strand cDNA Synthesis kit	Thermo Fisher Scientific	Cat# K1651
PureLink™ Genomic DNA Mini Kit	Thermo Fisher Scientific	Cat# K182001
Strep-Tactin® XT Spin Column Kit	IBA Lifesciences	Cat# 2-4151-000
Universal RNA Purification Kit	Roboklon	Cat# E3598
Deposited data		
Mass spectrometry proteomics data	ProteomeXchange Consortium (http://proteomecentral.proteomexchange.org/cgi/GetDataset?ID=PXD030501)	PXD: PXD030501
RNAseq analysis of H441 cells	NCBI Gene Expression Omnibus (https://www.ncbi.nlm.nih.gov/geo/query/acc.cgi?acc=GSE217895)	GEO: GSE217895
Experimental models: Cell lines		
A549	Sigma-Aldrich	Cat# 86012804-1VL
A549-Cas9 (SL504)	GeneCopoiea	Cat# SCL-76321-G2
A549-Cas9 p11-KO cells	This paper	N/A
A549-T/C	This paper	N/A
BEAS-2B	ATCC (The American Type Culture Collection)	Cat# CRL-9609™
H441	ATCC	Cat# CRM-HTB-174
HepG2	DSMZ (German Collection of Microorganisms and Cell Cultures)	Cat# ACC 180
Human Small Airway Epithelial (pAEC) Cells	Lonza	Cat# CC-2547
Mouse lung epithelial T7 cells	ECACC (The European Collection of Authenticated Cell Cultures)	Cat# 07021402
Experimental models: Organisms/strains		
Aspergillus fumigatus strain CEA17 Δ*akuB*^{KU80}	da Silva Ferreira et al.[65]	N/A
A. fumigatus strain Δ*hscA*	This paper	N/A

(*Continued on next page*)

Continued

REAGENT or RESOURCE	SOURCE	IDENTIFIER
A. fumigatus strain *hscA-gfp*	This paper	N/A
A. fumigatus strain *hscAc*	This paper	N/A
A. fumigatus strain *hscA-myc*	This paper	N/A
A. fumigatus strain *ccpA-gfp*	Voltersen et al.[26]	N/A
Oligonucleotides		
Forward and reverse primers for generation and verification of Δ*hscA* and *hscA-gfp*	This paper, Table S4	N/A
Forward and reverse primers for constructs	This paper, Table S4	N/A
Forward and reverse primers for qPCR detection	This paper and Lu et al.,[56] Table S4	N/A
ON-TARGETplus Human S100A10 siRNA SMARTpool	Horizon Discovery	Cat# L-011766-00-0005
ON-TARGETplus GAPDH Control Pool – human	Horizon Discovery	Cat# D-001830-10-05
ON-TARGETplus Non-targeting Control Pool	Horizon Discovery	Cat# D-001810-10-05
Recombinant DNA		
A. fumigatus strain transformation: pLJ-Hsp70-Myc	Jia et al.[24]	N/A
A. fumigatus strain transformation: pLJ-HscA-Comp	This paper	N/A
A. fumigatus strain transformation: pLJ-HscA-Myc	This paper	N/A
A. fumigatus strain transformation: pTH-1	Lapp et al.[66]	N/A
Cloning vector: pJET1.2	Thermo Fisher Scientific	Cat# K1231
Generation of A549-T/C: pSpCas9 (BB)-2A-Puro (PX459) V2.0	Ran et al.[69]	Cat# 62988; RRID: Addgene_62988
Generation of A549-T/C: pLJ-064	This paper	N/A
HCP216549-SG01-3 for generation of p11-KO cell line	GeneCopoiea	Cat# HCP216549-SG01-3
Protein expression construct: pnEATST-AfHscA	This paper	N/A
Protein expression construct: pnEATST-AfHsp70	This paper	N/A
Software and algorithms		
Chromeleon 7.2	Thermo Fisher Scientific	N/A
Graphpad Prism 7.0	GraphPad	https://www.graphpad.com/
Imaging Fusion16	Vilber Lourmat	https://www.vilber.com/
Proteome Discoverer 2.4	Thermo Fisher Scientific	N/A
QExactive HF Tune 2.8	Thermo Fisher Scientific	N/A
Xcalibur 4.0	Thermo Fisher Scientific	N/A
Zeiss ZEN software (black edition)	Zeiss	N/A
Zeiss ZEN software 3.0 (blue edition)	Zeiss	N/A
Other		
Anti-Biotin Micro-Beads Ultra-Pure	Miltenyi Biotec	Cat# 130-105-637
Dynabeads™ Protein G	Thermo Fisher Scientific	Cat# 10003D
GFP-trap magnetic agarose	ChromoTek	Cat# gtma-20
Dissociation buffer	Thermo Fisher Scientific	Cat# 13151014
FcR blocking reagent	Miltenyi Biotec	Cat# 130-059-901
FetalClone III serum (FCS)	Cytiva	Cat# SH30109
GlutaMAXTM-I	Gibco	Cat# 35050-038
iBlot™ 2 Gel Transfer Device	Thermo Fisher Scientific	Cat# IB21001
iBlot™ 2 Transfer Stacks, PVDF, mini	Thermo Fisher Scientific	Cat# IB24002
Latex beads, fluorescent red, 2.0 μm mean particle size	Sigma-Aldrich	Cat# L3030
Latex beads, fluorescent yellow-green, 1.0 μm mean particle size	Sigma-Aldrich	Cat# L1030
Latex beads, 3.0 μm mean particle size	Sigma-Aldrich	Cat# LB30
Latex beads, magnetic, 1.0 μm mean particle size	Sigma-Aldrich	Cat# 75597

(*Continued on next page*)

Continued

REAGENT or RESOURCE	SOURCE	IDENTIFIER
LHC-9 medium	Gibco	Cat# 12680013
Lipofectamine 3000 transfection reagent	Thermo Fisher Scientific	Cat# L3000001
NuPAGE™ 4%–12% Bis-Tris Gels	Thermo Fisher Scientific	Cat# NP0322BOX
Opti-MEM™ I Reduced Serum Medium, no phenol red	Thermo Fisher Scientific	Cat# 11058021
Red blood cell lysis buffer	Roche	Cat# 11814389001
SAGM™ Small Airway Epithelial Cell Growth Medium BulletKit™	Lonza	Cat# CC-3118
Transfer membrane ROTI®Nylon plus	Carl ROTH	Cat# K058.1

RESOURCE AVAILABILITY

Lead contact

Further information and requests for resources and reagents should be directed to and will be fulfilled by the lead contact, Axel A. Brakhage (axel.brakhage@leibniz-hki.de).

Materials availability

- All materials within the paper are available from the corresponding author upon reasonable request.
- This study did not generate new unique reagents.

Data and code availability

- The mass spectrometry proteomics data have been deposited to the ProteomeXchange Consortium via the PRIDE[64] partner repository with the dataset identifier PXD: PXD030501. The RNAseq data of H441 cells have been deposited at NCBI Gene Expression Omnibus (GEO: GSE217895). See also the key resources table.
- This paper does not report original code.
- Any additional information required to reanalyze the data reported in this work paper is available from the lead contact upon request.

EXPERIMENTAL MODEL AND SUBJECT DETAILS

Cell culture and reagents

Human lung epithelial A549 cells (Cat# 86012804-1VL, Sigma-Aldrich) and human distal lung epithelial H441 cells (Cat# ATCC-CRM-HTB-174D, LGC) were cultured in F-12K Nut Mix medium (Kaighn's modification, Gibco) supplemented with 10% (v/v) artificial fetal calf serum (FCS) (HyClone FetalClone III serum, Cytiva). T7 mouse type-II alveolar epithelial cells (Cat# 07021402, ECACC) were cultured in F-12K Nut Mix medium supplemented with 5% (v/v) artificial FCS and with 0.5% (v/v) Insulin-Transferrin-Selenium (Thermo Fisher Scientific). BEAS-2B cells (Cat# CRL-9609, ATCC) were cultured in LHC-9 serum free medium (Thermo Fisher Scientific) in flasks precoated with LHC-9 medium supplemented with 0.01 mg/mL bovine fibronectin (Thermo Fisher Scientific), 0.03 mg/mL bovine collagen type I (Sigma-Aldrich) and 0.01 mg/mL BSA (Sigma-Aldrich). HepG2 cells (Cat# ACC 180, DSMZ) were cultured in RPMI-1640 medium supplemented with 10% (v/v) artificial FCS. A549 cells stably expressing Cas9 (Cat# SL504, GeneCopoiea) were cultured as mentioned above for A549 cells, but with addition of 800 μg/mL hygromycin (InvivoGen) as selection marker. The primary human airway epithelial (pAEC) cells (Cat# CC-2547, Lonza) were cultured in SAGM Small Airway Epithelial Cell Growth Medium BulletKit (Lonza). All cells were cultivated at 37°C and 5% (v/v) CO_2.

Fungal strains and cultivation

All strains used in this study are listed in key resources table. *A. fumigatus* conidia from WT and knockout strains were collected in water from *Aspergillus* minimal medium (AMM) agar plates after 5 days of growth at 37°C, and were counted using a CASY Cell Counter, as previously described.[24] For germination assays, 10^9 *A. fumigatus* resting conidia were incubated at 37°C in RPMI-1640 (GIBCO) to produce swollen conidia (4 h), germlings (8 h), and hyphae (14 h), as described previously.[24] For conidia production assay, 10^5 conidia were spread on AMM agar plates. After incubation at 37°C for 5 days, conidia were collected in 10 mL water and counted using CASY Cell Counter. For determination of their susceptibility to stressors, serial 10-fold dilutions of conidia ranging from 10^5 to 10^2 in 1 μL H_2O were spotted onto AMM agar plates containing 30 μg/mL Congo red, 1 mM 1,4-dithiothreitol, 10 μg/mL tunicamycin, 0.01% (w/v) SDS, or 300 μg/mL CFW. Fungal growth was monitored over time and images were collected before

overgrowth of the agar plates. For infection assays, *A. fumigatus* conidia were collected in water from malt agar (Sigma-Aldrich) plates respectively after 7 days of growth at room temperature (22°C). All conidia were harvested in sterile, double-distilled water.

METHOD DETAILS

Strain construction, Southern and Northern blot analysis

A split marker PCR strategy was used to replace the *hscA* gene (AFUB_083640) with the hygromycin B phosphotransferase gene (*hph*) in protoplasts from *A. fumigatus* strain CEA17 Δ*akuB*^{KU80}.[65] Briefly, a 1,085 base pairs (bp) upstream DNA fragment and a 986 bp downstream DNA fragment were amplified from *A. fumigatus* genomic DNA by high-fidelity PCR using primers HscA-P1, HscA-P2 and HscA-P3, HscA-P4. The two generated DNA fragments were fused with the *hph* cassette (HYG-F and HYG-R) resulting in a 4,809 bp DNA fragment by 3-fragment fusion PCR. A similar strategy was used to generate the *hscA-gfp* strain. A 4,984 bp fragment containing a 1,046 bp 3′ region (without TAA, using primers HscA-P5 and HscA-P6) of *hscA*, a *gfp-ptrA* cassette (using primers PtrA-F, PtrA-R and plasmid pTH1[66] as template), and a 1,031 bp downstream region (using primers HscA-P7 and HscA-P8) of *hscA* was generated. The *gfp-ptrA* cassette was in-frame fused to the *hscA* 3′ region. Then, the fragment was used for transformation of *A. fumigatus* protoplasts.

To complement the Δ*hscA* mutant, the intact *hscA* open reading frame, including 1,175 bp of upstream sequence and 683 bp of downstream sequence was amplified from genomic DNA by high-fidelity PCR using primers HscA-Com-F and HscA-Com-R. The resulting DNA fragment was cloned into plasmid pTH1[66] which was digested with *Kpn*I and *Not*I to obtain plasmid pLJ-HscA-Comp. To generate plasmid pLJ-HscA-Myc, a DNA fragment containing 1,175 bp of upstream sequence and *hscA* without TAA was amplified from genomic DNA by high-fidelity PCR using primers HscA-Com-F and HscA-Myc-R. The DNA fragment was then inserted into plasmid pLJ-Hsp70-Myc[24] which was digested with *Kpn*I and *Hin*dIII. Protoplasts of the Δ*hscA* mutant were transformed with plasmids pLJ-HscA-Comp or pLJ-HscA-Myc to generate the respective *A. fumigatus* strains *hscA*c and *hscA-myc*.

For Southern blot analysis, chromosomal DNA of *A. fumigatus* was digested with *Bam*HI. DNA fragments were separated in an agarose gel and blotted onto nylon membranes (Carl ROTH). Northern blot analysis was performed as described previously.[67] Total RNA was extracted using a universal RNA purification kit (Roboklon). 10 μg of RNA was separated on a denaturing agarose gel, rRNA bands served as loading control. RNA was then transferred onto positively charged nylon membranes (Carl ROTH). Probes were labeled with digoxigenin (DIG) by addition of DIG-11-dUTP (Jena Bioscience) to the PCR mixture. Probe A, synthesized with primers HscA-P8 and oJLJ19-18, probe B, synthesized with primers oJLJ19-45 and oJLJ19-46, were used for Southern blot analysis to verify the *hscA* mutant strain. Probe B was also used for Northern blot analysis to detect *hscA* expression. Probe C was synthesized using primers oJLJ19-33 and oJLJ19-42 to probe *hsp70* mRNA. Probes were detected with an anti-DIG antibody (Roche). Primers used were listed in Table S4.

Isolation of CD45$^+$ cells from human lung tissues

Healthy human lung tissue was collected during lung surgery on cancer patients (approved by the ethical committee of the Friedrich Schiller University in Jena, Registration number: 2020-1894 1-Material). Tissue was aseptically removed from the non-tumor affected edges of resected lung wedges or lobes and stored in sterile PBS (PBS) at 4°C. Tissues were processed between 4 and 24 h after surgery. One cm^3 of the tissue was cut by surgical blade and chopped to smaller pieces by scissors. Enzyme mixture 1 (2 mL TrypLE Trypsin + 0.5 mL Dispase + 3 μL Elastase) or enzyme mixture 2 (2.5 mL Dispase + 3 μL Elastase + 5 μL DNase) was added to the falcon tube together with tissue and incubated for 30 min at 37°C in a water bath. After incubation, the mixture was filtered through 70 μm and 30 μm cell strainer and washed thoroughly by DMEM/F12 medium (Gibco) and centrifuged with 300 × *g* for 10 min at 4°C. The cell pellet was resuspended in 2 mL Red blood cell lysis buffer (Roche) with 5 μL DNase (1 mg/mL), incubated for 2 min at room temperature and diluted with 6 mL DMEM/F12 medium. After centrifugation at 300 × *g* for 5 min at 4°C, cells were resuspended in 500 μL PEB buffer (autoMACS rinsing solution (Miltenyi Biotec) + 5 μL DNase + 0.5% (v/v) heat-inactivated FCS) with 10 μL FcR blocking reagent (Miltenyi Biotec), 10 μL biotin labeled anti-CD45 antibody (Miltenyi Biotec). After incubation for 30 min at 4°C, cells were washed with 5 mL DMEM/F12 medium and centrifuged with 300 × *g* for 10 min at 4°C. The cell pellet was resuspended in 70 μL PEB buffer with 20 μL anti-biotin magnetic beads and incubated at 4°C for 15 min. After another wash with 5 mL media, cells were resuspended in 1 mL PEB buffer and proceeded to magnetic separation on autoMACSpro separator (Miltenyi Biotec) with Possels program. Cells were counted with a LUNA-FL cell counter (Logos Biosystems) and their viability was controlled by Trypan Blue staining (1:1 cell suspension + Trypan Blue). Cells (8 × 10^4) were seeded on fibronectin (bovine, 0.1 mg/mL) coated Millicell EZ $_{SLIDE}$ 8-Well (Merck) in 300 μL media/well (RPMI + 10% (v/v) FCS + 1% (w/v) ultraglutamine + 1% (w/v) Pen/Strep + 1% (w/v) HEPES + 1% (w/v) Na-pyruvate + 1% (v/v) MEM NEAA + 0.1% (v/v) mercaptoethanol).

Isolation of PMNs and peripheral blood mononuclear cells from human blood

Human polymorphonuclear leukocytes (PMNs) and peripheral blood mononuclear cells (PBMCs) were isolated from buffy coats provided by the Jena University Hospital. The blood was diluted 1:8 with pre-warmed PBS without calcium and magnesium. Twenty milliliters of the solution were carefully layered onto (avoiding any mixing) 20 mL (1:1, v/v) of PolymorphPrep solution (Progen) and centrifuged at room temperature for 35 min at 500 × *g* for gradient separation. Both cell-containing rings indicative of PBMCs and PMNs ring were transferred into new falcons with 10 mL PBS. After adding PBS to a final volume of 50 mL, the cells were centrifuged for 10 min at 300 × *g*. Cell pellets were resuspended in 3 mL ACK lysis buffer (Gibco) to reduce the contamination of

erythrocytes. Followed by another fill-up with PBS to 50 mL and centrifugation step, cells were finally resuspended in RPMI medium and counted with a Luna automated cell counter (Logos Biosystems). PBMCs were differentiated for 5 days by adding 20 ng/mL of human M-CSF (Peprotech) to the cultivation medium.

Knockdown and knockout of human p11 gene

ON-TARGETplus Human S100A10 siRNA SMARTpool (Horizon Discovery) was used to knockdown p11 expression. Briefly, 50 μL per well of transfection solution containing 125 nM siRNA and DharmaFECT (1:100) in serum-free F-12 K Nut Mix medium was added to 8-well slides and incubated for 25 min. 4×10^4 cells in 250 μL F-12 K Nut Mix medium supplemented with 10% (v/v) FCS were then added to the wells and incubated at 37°C with 5% (v/v) CO_2. The medium was replaced by fresh complete medium on the next day and cells were analyzed on day 3 after transfection by immunoblotting. The A2t inhibitor A2ti-1 (2-[4-(2-ethylphenyl)-5-*o*-tolyloxymethyl-4H-[1,2,4]triazol-3-ylsulfanyl]acetamide, MedChemExpress) was dissolved in DMSO. A549 cells seeded at 3×10^4 cells/well were incubated in an 8-well slide at 37°C with 100 μM of A2ti-1 for 2 days before incubation with *A. fumigatus* conidia. In control experiments, cells were treated with DMSO at the same concentrations used for A2ti-1 delivery.

To generate p11-KO cells, A549-Cas9 (GeneCopoiea) cells were transformed with a mixture of sgRNA plasmids, including HCP216549-SG01-3-10-A, HCP216549-SG01-3-10-B, and HCP216549-SG01-3-10-C (GeneCopoiea, 0.5 μg of each plasmid), using Lipofectamine 3000 reagent (Thermo Fisher Scientific). Colonies derived from single cells were screened for p11 knockout by Western blot and immunofluorescence analysis. The p11-KO cell line was further confirmed by DNA sequencing. Briefly, the fragment containing the first CDS of p11 gene was PCR amplified from the genomic DNA of p11-KO cells using primers oJLJ21-25 and oJLJ21-26 (Table S4). The PCR product was inserted into the cloning vector pJET1.2 (Thermo Fisher Scientific) and sequenced with primer oJLJ21-25 or oJLJ21-26 (Figure S3A).

Gene editing for creating a single-base substitution at the rs1873311 SNP locus

The genotype of A549 (T/T, homozygous), pAEC (T/T, homozygous), and H441 (T/C, heterozygous) cells, at the SNP rs1873311 locus was confirmed by sequencing of PCR fragment generated using primers oJLJ21-41 and oJLJ21-42. To generate an isogenic T/C cell line of A549, we employed the CRISPR/Cas9-mediated single nucleotide mutation method as described previously.[68] First, we generated plasmid pLJ-064, which expresses the gRNA targeting the "TCCCTGAAGAACTTCAGTTTTGG" sequence close to the rs1873311 locus. To generate plasmid pLJ-064, a 1,759 bp DNA fragment containing the "TCCCTGAAGAACTTCAGTTT" sequence was amplified from pSpCas9(BB)-2A-Puro (PX459) V2.0 (Addgene plasmid # 62988), a gift from Feng Zhang,[69] by high-fidelity PCR using primers oJLJ22-08, oJLJ22-09, oJLJ21-34, and oJLJ21-35. The resulting DNA fragment was then cloned into plasmid pSpCas9(BB)-2A-Puro (PX459) V2.0.

For transfection, 1×10^5 A549 cells were cultivated in 24-well plate overnight at 37°C with 5% (v/v) CO_2. Then cells were transfected with 0.5 μg of sgRNA plasmid (pLJ-064) and 100 pmol of oJLJ21-43 (single-stranded oligo DNA with 74 nucleotides, Table S4) as template using Lipofectamine 3000 reagent in Opti-MEM I Reduced-Serum Medium (Thermo Fisher Scientific). After 8–10 h of incubation at 37°C with 5% (v/v) CO_2, the transfection medium was exchanged by pre-warmed complete growth medium. At 24 h post transfection, puromycin was added at a concentration of 0.75 μg/mL. After another 24 h of cultivation, cells were transferred at 1 cell/well in 96-well plates for single colonies and further cultivated for 20–30 days until colonies had formed. DNA of the colonies was extracted using PureLink Genomic DNA Mini Kit (Thermo Fisher Scientific). The genotypes of the colonies were analyzed by cutting the PCR fragments (primers oJLJ21-41 and oJLJ21-42) with *Nhe*I. PCR fragments of the positive clones were further analyzed by DNA sequencing (Figure S6B). The T/C heterozygous clone 6 was named as A549-T/C and was further incubated with *A. fumigatus* conidia for phenotype analysis. The T/T homozygous clone 2 and clone 4 were used as control and named A549-T/T.

Biotinylation of surface proteins

The surface biotinylation method was applied as described previously.[24] Briefly, the fungal conidia and mycelium were washed three times with PBS (pH 7.4), and then incubated in 5 mL of PBS containing 5 mg EZ-Link Sulfo-NHS-LC-Biotin (Thermo Fisher Scientific) for 30 min at 4°C. The reaction was terminated by addition of two volumes of 100 mM Tris-HCl (pH 7.4), and the reaction mixture was incubated further for 30 min. Then the samples were washed another three times with PBS. After addition of 1 mL of PBS containing protease inhibitor cocktail (Roche) and 500 μL of 0.5-mm-diameter glass beads (Carl ROTH), conidia, germlings, and hyphae were disrupted using a FastPrep homogenizer with the following settings: 6.5 m/s, 3 times for 30 s each time. The samples were then centrifuged with 16,000 × *g* for 10 min at 4°C. Supernatants were collected and their total protein concentration was determined by Pierce Coomassie Plus (Bradford) Protein Assay (Thermo Fisher Scientific).

Production of antibody against HscA

To produce an antibody against HscA, two synthesized antigen peptides Cys-TMSLKLKRGNKEKIESALSDA and Cys-DYKKKELALKRLITKAMATR (Figure S1C) were conjugated to KLH carrier and used for raising polyclonal antibodies in rabbits (ProteoGenix, France). The detection of HscA using polyclonal antibodies was performed by Western blot analysis of the protein extracts of *A. fumigatus* WT, Δ*hscA*, *hscA*c, and *hscA-myc* (Figure S1D).

Western blotting

For detection of proteins by Western blots, whole protein extracts from fungus or host cells were separated on NuPAGE 4%–12% Bis-Tris Gels (Invitrogen) and transferred to 0.2-μm pore size PVDF membranes (Invitrogen) using the iBlot 2 Gel Transfer Device (Thermo Fisher Scientific). Membranes were blocked by incubation in 5% (w/v) milk powder or 1 × Western Blocking Reagent (Roche) in Tris-buffered saline and 0.1% (v/v) Tween 20 for 1 h at room temperature. Primary antibody incubation was carried out at 4°C overnight. The primary antibodies including the purified rabbit polyclonal anti-HscA antibody (this study, 1:10,000), mouse monoclonal anti-biotin antibody (Thermo Fisher Scientific, 1:2,000 dilution), mouse monoclonal anti-Hsp70 antibody (Thermo Fisher Scientific, 1:1,000 dilution), rabbit polyclonal anti-Myc antibody (Cell Signaling Technology, 1:5,000 dilution), mouse monoclonal anti-Strep antibody (IBA, 1:1,000 dilution), mouse monoclonal anti-GFP antibody (Santa Cruz, 1:1,000 dilution), mouse monoclonal anti-p11 antibody (BD, 1:1,000 dilution), rabbit polyclonal anti-p11 antibody (1:1,000 dilution), rabbit monoclonal anti-AnxA2 antibody (Cell Signaling Technology, 1:2,000 dilution), rabbit monoclonal anti-β-actin antibody (Cell Signaling Technology, 1:2,000 dilution), and mouse monoclonal anti-GAPDH antibody (Proteintech, 1:2,000 dilution) were used. Hybridization of primary antibody with an HRP-linked anti-mouse IgG (Cell Signaling Technology) or HRP-linked anti-rabbit IgG (Abcam) was performed for 1 h at room temperature. Chemiluminescence of HRP substrate (Millipore) was detected with a Fusion FX7 system (Vilber Lourmat, Germany).

Production of purified recombinant HscA and Hsp70

The coding sequences of *hscA* (with primers AfhscANdeIf and AfhscABamHIr) and *hsp70* (with primers Afhsp70NdeIf and Afhsp70BamHIr) were PCR amplified from *A. fumigatus* cDNA. The generated DNA fragments were cloned into the vector pnEATST (modified pET15b vector encoding an N-terminal Twin-Strep-tag followed by a tobacco etch virus protease site). Recombinant proteins were produced in *E. coli* BL21 (DE3) cells (New England Biolabs) by auto induction (Overnight Express Instant TB Medium, Novagen) at 25°C. Bacterial cells were then harvested by centrifugation (10,500 × *g*) and stored at -80°C. Frozen bacterial cells were resuspended in lysis buffer (100 mM Tris/HCl, 150 mM NaCl, 1 mM AEBSF, 0.5% (v/v) BioLock, pH 8.0) and disrupted at 1,000 bar using a high-pressure homogenizer (Emulsiflex C5, Avestin). After centrifugation (48,000 × *g*) and filtration of the lysates through a 1.2 μm membrane, recombinant proteins were purified by affinity chromatography using a 5 mL Strep-TactinXT superflow high capacity column (IBA). Proteins were eluted from the column with biotin elution buffer (100 mM Tris/HCL, 150 mM NaCl, 1 mM EDTA, 50 mM biotin, pH 8.0). A HiPrep 26/10 Desalting column (Cytiva) was used to transfer fractionated HscA and Hsp70 peaks to storage buffer (20 mM HEPES, 150 mM NaCl, 5 mM $MgCl_2$, 10% (v/v) glycerol, 1 mM TCEP, pH 7.5).

Proteomics analysis

To identify the protein(s) from A549 cells binding to HscA, we incubated 10 mg of A549 cell protein extracts with 50 μg purified recombinant HscA protein for 2 h at 4°C. Proteins were then purified using Strep-TactinXT spin column kit (IBA). Reduction and alkylation of cysteine thiols was performed by addition of 5 mM tris(2-carboxyethyl)phosphine and 6.25 mM 2-chloroacetamide (final concentrations) followed by incubation at 70°C for 30 min. Subsequently, proteins were dried in a vacuum concentrator (Eppendorf) and resolubilized in 50 μL of 100 mM TEAB. Proteolytic digestion was carried out with a trypsin/Lys-C mixture (Promega) incubated for 18 h at 37 °C at a protein to protease ratio of 25:1. Tryptic peptides were evaporated in a vacuum concentrator until dryness, resolubilized in 25 μL of 0.05% (v/v) trifluoroacetic acid in 98:2 H_2O/acetonitrile (v/v) and filtrated through a 0.2 μm spin filter (Merck Millipore Ultra-free-MC, hydrophilic PTFE) at 14,000 × *g* for 15 min. Filtrated peptides were transferred into HPLC vials and analyzed by LC-MS/MS.

LC-MS/MS analysis was performed on an Ultimate 3000 nano RSLC system connected to a QExactive HF mass spectrometer (both Thermo Fisher Scientific, Waltham, MA, USA). Peptide trapping for 5 min on an Acclaim Pep Map 100 column (2 cm × 75 μm, 3 μm) at 5 μL/min was followed by separation on an analytical Acclaim Pep Map RSLC nano column (50 cm × 75 μm, 2μm). Mobile phase gradient elution of eluent A (0.1% (v/v) formic acid in water) mixed with eluent B (0.1% (v/v) formic acid in 90:10 acetonitrile/water) was performed using the following gradient: 0 min at 4% B, 5 min at 8% B, 20 min at 12% B, 30 min at 18% B, 40 min at 25% B, 50 min at 35% B, 57 min at 50% B, 62–65 min at 96% B, 65.1–90 min at 4% B. Positively charged ions were generated at spray voltage of 2.2 kV using a stainless steel emitter attached to the Nanospray Flex Ion Source (Thermo Fisher Scientific). The quadrupole/orbitrap instrument was operated in Full MS/data-dependent MS2 Top15 mode. Precursor ions were monitored at *m/z* 300–1,500 at a resolution of 60,000 full width at half maximum (FWHM) using a maximum injection time (ITmax) of 100 ms and an AGC (automatic gain control) target of 1×10^6. Precursor ions with a charge state of z = 2–5 were filtered at an isolation width of *m/z* 2.0 amu for further HCD fragmentation at 30% normalized collision energy. MS2 ions were scanned at 15,000 FWHM (ITmax = 80 ms, AGC = 2×10^5) using a fixed first mass of *m/z* 120 amu. Dynamic exclusion of precursor ions was set to 20 s. The LC-MS/MS instrument was controlled by Chromeleon 7.2, QExactive HF Tune 2.8 and Xcalibur 4.0 software.

Tandem mass spectra were searched against the UniProt databases (2020/07/13; YYYY/MM/DD) of *Homo sapiens* (https://www.uniprot.org/proteomes/UP000005640) and *Neosartorya fumigata* (*A. fumigatus*) Af293 (https://www.uniprot.org/proteomes/UP000002530) using Proteome Discoverer (PD) 2.4 (Thermo Fisher Scientific) and the algorithms of Mascot 2.4.1 (Matrix Science, UK), Sequest HT (version of PD2.4), MS Amanda 2.0, and MS Fragger 2.4. Two missed cleavages were allowed for the tryptic digestion. The precursor mass tolerance was set to 10 ppm and the fragment mass tolerance was set to 0.02 Da. Modifications were defined as dynamic Met oxidation, protein N-term acetylation and Met-loss as well as static Cys carbamidomethylation. A strict false discovery rate (FDR) < 1% (peptide and protein level) and a search engine score of > 30 (Mascot), > 4 (Sequest HT), > 300 (MS Amanda), or > 8 (MS Fragger) were required for positive protein hits. The Percolator node of PD2.4 and a reverse decoy database

was used for q value validation of spectral matches. Only rank 1 proteins and peptides of the top scored proteins were counted. Label-free protein quantification was based on the Minora algorithm of PD2.4 using the precursor abundance based on intensity and a signal-to-noise ratio > 5. Relative abundance of protein was calculated as PSM (peptide spectrum matches)/protein length/total PSM.

Infection experiments of cells

For infection experiments, *A. fumigatus* conidia were collected in water from malt agar plates after 7 days of growth at room temperature (22°C). A549, H441, pAEC, and T7 epithelial cells were seeded in Millicell EZ $_{SLIDE}$ 8-Well at a density of 3×10^4 cells per well and incubated overnight at 37°C in a humidified chamber with 5% (v/v) CO_2. Conidia were added at a MOI of 10. Recombinant proteins, including rHscA and rHsp70, were added at a concentration of 10 μg/mL. Synchronization of infection was achieved by centrifugation for 5 min at 100 × *g*. For immunofluorescence and microscopy, infection of epithelial cells was allowed to proceed for 8 h, infection of lung isolated $CD45^+$ cells was proceeded for 3 h, and infection of PMNs and PBMCs was proceeded for 2 h at 37°C in the humidified chamber with 5% (v/v) CO_2. For Western blot analysis of p11 protein expression, cells were seeded in a 12-well plate at a density of 5×10^5 cells per well. Conidia or IFN-γ (Gibco, 50 ng/mL) was added to cells and incubated for 1, 2, or 4 h at 37°C in the humidified chamber with 5% (v/v) CO_2. For lactate dehydrogenase (LDH) release assay, A549 cells were seeded in a 24-well plate at a density of 2×10^5 cells per well. After an incubation for 20 h, LDH activity was measured using the CyQuant LDH cytotoxicity assay (Thermo Fisher Scientific) following the manufacturer's instructions.

Immunofluorescence and microscopy

To stain *A. fumigatus* proteins binding to host cells, living A549, H441, HepG2, and T7 cells were incubated with 20 μg *A. fumigatus* protein extracts or 2 μg purified rHscA or rHsp70 protein at room temperature for 1 h. After three times of washing with PBS, cells were stained with Alexa Fluor 488-conjugated streptavidin (Thermo Fisher Scientific) at room temperature for 1 h to detect biotinylated *A. fumigatus* surface proteins binding to host cells. To stain host cell binding of HscA-GFP protein, cells were incubated with a rabbit anti-GFP primary antibody (Abcam) for 2 h at room temperature and a secondary antibody for 1 h at room temperature in the dark. To stain host cell binding of purified rHscA protein, StrepMAB-Classic (IBA) was used to stain the cells.

To detect HscA-Myc on the surface of *A. fumigatus* conidia, the cell wall of germlings of WT and *hscA-myc* strains was stained with calcofluor white (CFW, 250 μg/mL) for 10 min. Then, the different morphotypes were stained with a mouse anti-Myc primary antibody (Cell Signaling Technology, 1:100 dilution) for 2 h at room temperature. The germlings were then incubated with a secondary antibody (goat anti-mouse IgG H&L, Thermo Fisher Scientific, 1:500 dilution) for 1 h at room temperature in the dark. For monitoring colocalization of HscA-Myc and p11, living A549 cells were incubated with 20 μg protein extracts from germlings of *hscA-myc* at room temperature for 1 h. Colocalization of HscA-Myc and p11 was indirectly detected using a rabbit anti-Myc antibody (Abcam, 1:100 dilution) and a mouse anti-p11 antibody (BD, 1:200 dilution). As a negative control, the mouse anti-p11 antibody was not added.

For staining of phagosomal markers, after infection with conidia, epithelial cells were first incubated with 250 μg/mL CFW for 10 min at room temperature, as described previously.[18] This way, CFW exclusively stained extracellular conidia. For detection of phagosomal markers in both PMNs and PBMCs, cells were incubated with CFW-labeled conidia for 2 h. After three washing steps with PBS, cells were fixed for 10 min with 3.7% (v/v) formaldehyde, membranes were permeabilized for 10 min with 0.1% (v/v) Triton X-100/PBS and blocked for 30 min with 1% (w/v) BSA/PBS. Cells were incubated with primary antibodies at 4°C overnight, followed by incubation with secondary goat anti-mouse IgG Alexa Fluor 488 or goat anti-rabbit IgG DyLight 633 (Thermo Fisher Scientific). To determine phagolysosomal acidification, 50 nM LysoTracker red DND-99 (Thermo Fisher Scientific) was added to A549 epithelial cells 4 h after infection. After another 4 h of incubation, cells were stained with CFW for 10 min, and fixed for 10 min with 3.7% (v/v) formaldehyde. To stain exocytosed conidia, *A. fumigatus* dormant conidia were incubated with A549 cells for 4 h to internalize conidia. Conidia outside of host cells were counter-stained with 250 μg/mL CFW for 10 min at 37°C. CFW was then removed by three times of washing with pre-warmed PBS. After another 4 h of incubation at 37°C, cells were subjected to immunostaining. Samples were visualized using a Zeiss LSM 780 confocal microscope or a Zeiss Axio Imager M2 microscope and processed with the Zeiss ZEN software.

For quantification, at least 10 individual images of host cells infected with *A. fumigatus* conidia were counted for each experiment of at least three biological replicates. The numbers of extracellular conidia attached to host cells, internalized conidia, phagosomes with positive markers, phagocytic cups, and host cells were counted. The association of conidia with cells was calculated as: (number of internalized conidia + number of conidia attached to the host cells)/number of host cells. The percentage of internalized conidia was calculated as follows: number of internalized conidia/(number of internalized conidia + number of conidia attached to the host cells) × 100. The percentage of phagosomes with a positive marker was calculated as follows: number of phagosomes with a positive marker/number of internalized conidia × 100. The percentage of $p11^+$ phagocytic cups was calculated as follows: number of $p11^+$ conidia attached to host cells/number of conidia attached to host cells × 100. The percentage of exocytosed conidia was calculated: number of attached conidia with a $Rab11^+$ phagocytic cup/number of total conidia × 100.

For live cell imaging, 5×10^4 A549 cells were cultured overnight in eight-well slides (ibidi) and were infected with *A. fumigatus* conidia at MOI = 5 for 4 h. The cells were then washed with pre-warmed medium and kept inside an incubation chamber at 37°C, 5% (v/v) CO_2 before carrying out live cell imaging. Confocal time lapse sequences were captured using a Zeiss LSM 780 confocal microscope using a Plan-Apochromat 20x/0.8 M27 objective lens. Images were generated with a 561 nm diode-pumped solid-state laser and collected by the transmitted light photomultiplier tube of the LSM 780 system. Images were collected for 4 h at 1–10 s intervals

as Z stacks with 2,000 nm Z spacing, recording 9–22 confocal slices at each time point. Images consisted of 1,024 by 1,024 pixels at a voxel size of 415 × 415 × 2,000 nm. Quantification of conidia which were exocytosed or transferred between cells were carried out by counting total internalized conidia per replicate.

Incubation of latex beads with cells

Latex beads were coated as previously described.[70] Briefly, 20 μL of bead solution were sequentially washed in 1 mL PBS and 1 mL coupling buffer (0.2 M Na_2HCO_3, pH 8.5 and 0.5 M NaCl), and were resuspended in 100 μL of coupling buffer. Purified rHscA and rHsp70 proteins were added in a concentration of 0.5 mg/mL. The suspensions were incubated at 37°C for 30 min. After adding 500 μL of coupling buffer, the suspensions were sonicated for 5 min. For blocking of beads, 500 μL of 10 mg/mL BSA (AppliChem) in coupling buffer was added and it was incubated at 37°C for 1 h. The beads were washed in 1 mL PBS with 10 mg/mL BSA and stored in 200 μL of PBS containing 2 mg/mL BSA at 4°C. Presence of recombinant proteins on the surface of coated beads was verified by detection of Strep tag using immunofluorescence microscopy (Figure 2K).

To quantify the association of latex beads with host cells, fluorescent latex beads (Sigma-Aldrich) coated with recombinant protein were added to A549 cells seeded in Millicell EZ $_{SLIDE}$ 8-Well at a density of 3×10^4 cells per well at MOI = 20. After 8 h of incubation at 37°C and 5% (v/v) CO_2, cells were washed three times with PBS and then fixed with 3.7% (v/v) formaldehyde. The slides were examined using immunofluorescence microscopy. The association index is calculated as number of latex beads per cell divided by the number of BSA-coated latex beads per cell.

To isolate host proteins associated with latex beads, we coated magnetic latex beads (Sigma-Aldrich, 1 μm mean particle size) with rHscA or rHsp70 respectively. The beads were incubated with A549 cells for 8 h at MOI = 20. After washing-off the unbound beads with PBS, cells were lysed by passing the cells through a 27G needle in homogenization buffer (250 mM sucrose, 3 mM imidazole, pH 7.4), as previously described.[38] After 5 times of washing with PBS, proteins associated with latex beads were eluted in NuPAGE LDS Sample Buffer (Thermo Fisher Scientific) and analyzed by Western blotting.

RNA isolation, sequencing, and analysis

RNA isolation from cells was performed using the Universal RNA purification Kit (Roboklon GmbH, Berlin, Germany). 5×10^5 of A549, A549-T/T, A549-T/C, and T7 cells were co-incubated with *A. fumigatus* conidia with an MOI = 10 for 4 h at 37°C and 5% (v/v) CO_2. Cells were lysed in 400 μL buffer RL containing 10% (v/v) β-mercaptoethanol. RNA was extracted following the manufacturer's protocol for cell culture RNA purification. cDNA was synthesized from RNA using the Maxima H Minus First Strand cDNA Synthesis Kit (Thermo Fisher Scientific). Real-time qPCR was performed using iTaq Universal SYBR Green Supermix (Bio-rad) on a QuantStudio3 real-time PCR system (Thermo Fisher Scientific) with the following thermal cycling profile: 95°C for 20 s, followed by 40 cycles of amplification (95°C for 5 s, 58°C for 34 s). 18s rRNA was used as an endogenous control for normalization.

For H441 cells with or without *A. fumigatus* infection, RNA sequencing was performed to compare the expression of the p11 gene. Four replicates for each sample were sequenced and analyzed by Biomarker Technologies GmbH (Münster, Germany). RNA sequencing data is publicly available at NCBI GEO (Accession number: GSE217895). The relative p11 mRNA level was calculated by comparing the log2-transformed FPKM (fragments per kilobase of exon model per million reads mapped) value.

Co-immunoprecipitation

One 182 cm^2-flask of 80% confluent A549 cells was incubated with 20 mg crude protein extract of *A. fumigatus* for 2 h at 37°C. After 5 times of washing with PBS, cells were incubated with 1 mM DSP (dithiobis(succinimidyl propionate), Thermo Fisher Scientific) at room temperature for 30 min. The reaction was quenched with 10 mM Tris-HCl (pH 7.4), and the cells were lysed in 500 μL of IP lysis buffer (Thermo Fisher Scientific) with protease inhibitor cocktail (Roche). The lysates were centrifuged with 16,000 × *g* for 10 min at 4°C. The HscA-GFP protein was precipitated with GFP-trap magnetic agarose (ChromoTek). The co-immunoprecipitation of p11, AnxA2, and HscA-GFP was analyzed by Western blotting.

Genetic association study

The genetic association study with IPA was performed in a total of 483 hematological patients of European ancestry undergoing allogeneic hematopoietic stem cell transplantation at Instituto Português de Oncologia, Porto, and at Hospital de Santa Maria, Lisbon and were enrolled in the IFIGEN study between 2009 and 2016. The demographic and clinical characteristics of the patients are summarized in Table S3. Cases of probable/proven IPA were identified according to the standard criteria from the European Organization for Research and Treatment of Cancer/Mycology Study Group (EORTC/MSG).[71] Patients diagnosed with "possible" invasive fungal infection or with a pre-transplant infection were excluded from the study. Approval for the IFIGEN study was obtained from the SECVS (no. 125/014), the Ethics Committee for Health of the Instituto Português de Oncologia - Porto, Portugal (no. 26/015), the Ethics Committee of the Lisbon Academic Medical Center, Portugal (no. 632/014), and the National Commission for the Protection of Data, Portugal (no. 1950/015). Experiments were conducted according to the principles expressed in the Declaration of Helsinki, and participants provided written informed consent.

SNP selection and genotyping

Genomic DNA was isolated from whole blood using the QIAcube automated system (Qiagen). SNPs were selected based on their ability to tag surrounding variants with a pairwise correlation coefficient r^2 of at least 0.80 and a minor allele frequency ≥ 5% using

publicly available sequencing data from the Pilot 1 of the 1000 Genomes Project for the CEU population. Genotyping was performed using KASPar assays (LGC Genomics) in an Applied Biosystems 7500 Fast Real-Time PCR system (Thermo Fisher Scientific), according to the manufacturer's instructions.

QUANTIFICATION AND STATISTICAL ANALYSIS

Statistical analysis was performed using Prism 7. Two-tailed unpaired or paired Student's *t* test, one-way ANOVA or RM one-way ANOVA followed by Tukey's multiple comparisons test were used for data analysis. Numbers in parentheses in Figures 2B, 2C, 3H, 3I, and 3J represent the total number of individual images quantified. For bar graphs showing the quantification of phagocytic cups or phagosomes, numbers at the bottom or top of bar graphs represent total phagocytic cups or phagosomes analyzed. The probability of IPA according to *S100A10* genotypes was determined using the cumulative incidence method and compared using Gray's test.[72] Cumulative incidences at 24 months were computed with the *cmprsk* package for R version 2.10.1,[73] with censoring of data at the date of last follow-up visit and relapse and death as competing events. All clinical and genetic variables achieving a p value $\leq$ 0.15 in the univariate analysis were entered one by one in a pairwise model together and kept in the final model if they remained significant ($p < 0.05$). Multivariate analysis was performed using the subdistribution regression model of Fine and Gray with the *crr* function for R.[74]